DEPOSITION SYSTEM FOR THIN LITHIUM NUCLEAR TARGETS

By

Chunsun Lei

A thesis submitted in partial fulfillment of the
requirements for the degree of

Bachelor of Science

Houghton University

May 2024

Signature of Author……
Department of Physics
May 3, 2024

……
Dr. Mark Yuly
Professor of Physics
Research Supervisor

……
Dr. Brandon Hoffman
Professor of Physics

DEPOSITION SYSTEM FOR THIN LITHIUM NUCLEAR TARGETS

By

Chunsun Lei

Submitted to the Department of Physics
on May 3, 2024 in partial fulfillment of the
requirement for the degree of
Bachelor of Science

Abstract

A system was developed to create Sn or Ag coated Li nuclear targets for ICF simulation and Target Normal Sheath Acceleration (TNSA) experiments. The purpose of these experiments is to develop ways to measure low energy light-ion cross sections using high-power, ultra-fast lasers. The Li targets were designed to have a ~50 nm thick coating over a 2 μm thick Li film to prevent the Li from reacting with air and water vapor. The films were produced in a $\sim 10^{-5}$ Torr evacuated deposition chamber. Approximate 15 A flowing one way through a diode circuit heated a stainless-steel boat holding a Li pellet to a thermocouple-measured temperature of nearly 400°C, evaporating the Li onto a 25 μm thick stainless-steel substrate. A current of up to 60 A flowing the opposite direction through another diode heated a molybdenum boat holding a Sn or Ag pellet, evaporating the metal and forming the thin coating over the Li. The film thicknesses were measured using Rutherford backscattering, a magnetic adhesion tester, and a home-made profilometer. To allow Li metal to be weighed and inserted onto the boat without oxidization, an Ar-filled glove box was constructed around the deposition chamber.

Thesis Supervisor: Dr. Mark Yuly
Title: Professor of Physics

This material is based upon work supported by the Department of Energy [National Nuclear Security Administration] University of Rochester "National Inertial Confinement Program" under Award Number(s) DE-NA0004144.

CONTENTS

TABLE OF FIGURES

Chapter 1

NUCLEAR TARGETS FOR SLICS

A deposition system was designed and built to produce nuclear targets for experiments that were done with the Short-Lived Isotope Counting System (SLICS). SLICS is a detector system made of plastic scintillators and electronic digitizers which has been developed at Houghton University to make fundamental nuclear measurements of light-ion reactions. Experiments have been conducted to test the SLICS in order to develop it into a standard diagnostic instrument at the Laboratory for Laser Energetics (LLE).

1.1. Thin Film Target for Nuclear Experiments on the SLICS

In order to make nuclear measurement with the SLICS detector, thin film targets are needed that can be activated by light-ion bombardment. Thin films refer to a layer of material with a thickness in the order of micrometers on the surface of a substrate. Thin films have various applications across different fields, including electronics, optics, coatings, and sensors. For the purpose of making the nuclear targets needed for the SLICS detector, a deposition technique was developed to satisfy the different requirements for thickness, materials, the number of layers, and the specific needs of each experiment.

1.1.1. Lithium Films to Simulate ICF Reaction Products

The SLICS detector was developed with the original goal of measuring light-ion cross sections using Inertial Confinement Fusion (ICF). The cross section is proportional to the probability of a nuclear reaction occurring. Cross section measurements can be used to test theoretical models for specific nuclear reactions. A particular driving interest for the SLICS is to measure low keV incident energy cross sections needed for stellar and big bang nucleosynthesis models, as there is a lack of experimental data for light ion cross sections at low keV energy. Cross sections are traditionally experimentally measured using accelerators

where incident charged particles are accelerated toward a target by electric fields. However, light ion cross sections at low keV energy are difficult to measure using the accelerator method because as the energy of incident particles decreases, the probability of interactions typically decreases.

A different approach for measuring light ion cross sections at low energy is ICF. ICF is the process of using lasers to heat and compress a capsule containing a macroscopic amount of fuel, typically a mixture of deuterium and tritium. As the fuel undergoes intense heating and compression, it becomes so hot and dense that thermo-nuclear reactions occur. Afterward, as the plasma expands and cools off, the gas containing reaction products could be trapped and the number of product nuclei counted to measure cross sections. Figure 1 shows possible light ion nuclear reactions that could be studied through using ICF with a doped target capsule.

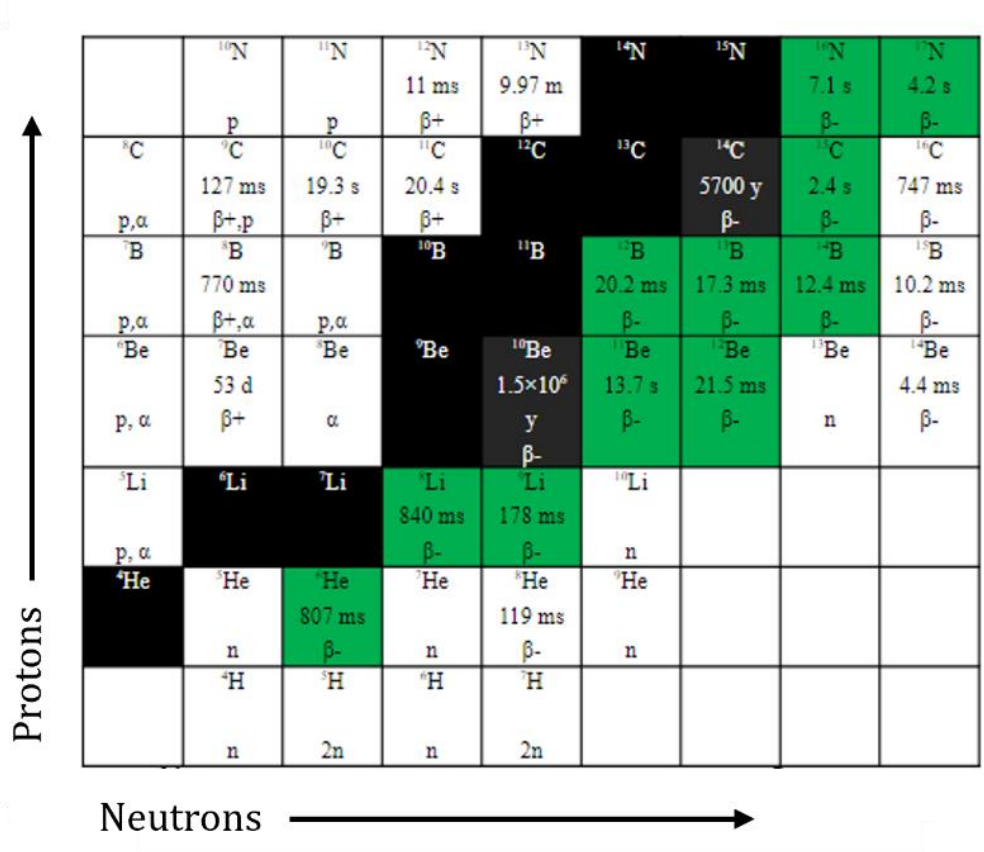

Figure 1. Chart of nuclides for light ion isotopes. The number of protons increases vertically, neutrons horizontally. The green isotopes can be

achieved via deuterium or tritium reactions with the black isotopes, and all decay via beta with half-life of about 10ms to 10s.

The black squares in Figure 1 are stable isotopes and the green squares are unstable isotopes that could be formed by deuterium or tritium induced reactions; all these beta decay with half-life in the range of 10 ms to 10 s. The SLICS was designed in such a way that it can be used to measure cross sections for reactions that lead to products shown in the green squares.

The SLICS detector consists of three major components that function together to trap the expanding gas and count the decays. The first component is the getter, which is an aluminum or titanium foil. The getter foil is placed in front of the plastic scintillators, trapping the outgoing vaporized product nuclei gas. The beta decay particles from the product nuclei travel through two layers of plastic scintillators of different thickness. The purpose of these different scintillators is to convert the energy deposited by the incoming decay particles into light pulses, which travel down a light guide to a photomultiplier tube (PMT). The light guide directs the light pulses into the PMT which converts light into current pulses. The third component is the digitizer which digitizes and saves all the pulses from the scintillators.

During the summer of 2022, an experiment used thin lithium targets to simulate the process of trapping and detecting ^{8}Li decay from the $^{7}\mathrm{Li}(\mathrm{d},\mathrm{p})^{8}\mathrm{Li}$ reaction in an after ICF implosion [1]. Lithium was chosen as the nuclear target because $^{7}\mathrm{Li}(\mathrm{d},\mathrm{p})^{8}\mathrm{Li}$ is one of the reactions of interest in Figure 1 with the largest cross section. The simulation utilized SUNY Geneseo's Pelletron accelerator to activate a lithium nuclear target which was then rapidly evaporated, trapped, and detected as shown in Figure 2. Throughout the entire experiment, the lithium nuclear targets were protected from air to prevent oxidization. They were kept either in vacuum or in an argon environment during transportation, and they were loaded into the argon-flushed experiment chamber. The thin lithium film nuclear target was held in the center of the experiment vacuum chamber. The deuteron beam from the accelerator entered the vacuum chamber through a connecting port. The deuteron beam was directed onto the lithium film and then a large electrical current heated the substrate to evaporate the reaction products to simulate the outgoing reaction product gas from the ICF implosion.

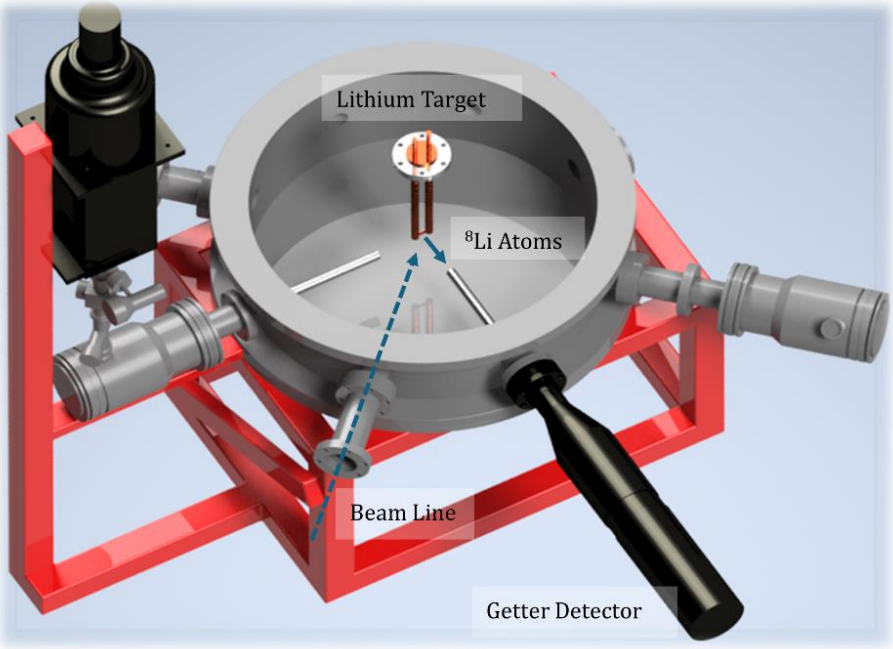

Figure 2. Overview of the ICF simulation setup. The lithium target was placed in the center of the chamber, where it was struck by a deuteron beam from the accelerator. The getter detector, which is part of the SLICS was placed near the nuclear target to trap, detect, and count the decay from the reaction product.

1.1.2. Coated Lithium Films for TNSA Experiment

An experiment conducted during the summer of 2023 which used lithium nuclear targets was conducted using the Multi-Terra Watt (MTW) laser at the Laboratory for Laser Energetics (LLE), where the high energy short pulse laser was used to study the $^{7}\mathrm{Li}(\mathrm{d},\mathrm{p})^{8}\mathrm{Li}$ reaction using Target Normal Sheath Acceleration (TNSA) [2]. TNSA is a process of using a short pulse, high energy laser to accelerate charged particles that can then be used as the incident particles to study nuclear reactions at energies up to tens of MeV. The TNSA process is shown in Figure 3, where the incoming laser hits and heats up the laser target forming a plasma. The electrons of the target are blown away, creating an electric field which accelerates the charged ions on the surface in the direction normal to the surface.

This experiment was conducted to test the feasibility of using the SLICS to measure MeV energy light ion reactions using TNSA rather than a traditional accelerator. The main

difference between TNSA and a traditional accelerator experiment is that TNSA makes it possible to generate all the reaction products in one short burst, as all the charged particles are accelerated toward the nuclear target at once, whereas a traditional accelerator generates a stream of charged particle. This difference can be advantageous for an activation experiment in which the product nuclei are decaying while they are also being formed by the ions in the beam of an accelerator. The overview of the experiment is shown in Figure 4. The incoming laser pulse was directed onto a deuterated polyethylene laser target through the combination of a redirection and concave mirror, then TNSA caused the deuterons to accelerate away from the laser target toward the nuclear target which was placed upstream of the detector. Once reaction products were formed through $^{7}Li(d, p)^{8}Li$, the beta particles from the decay of ^{8}Li were counted by the SLICS detector.

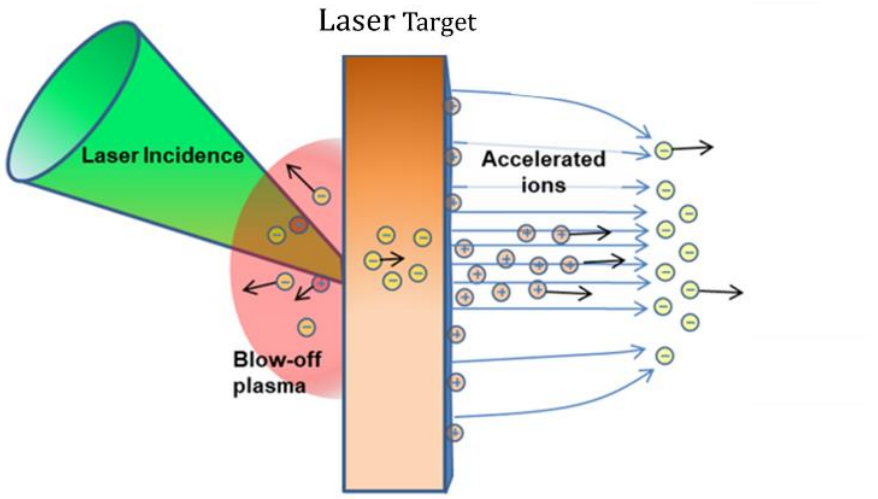

Figure 3. Overview of the TNSA process. The Incoming laser hits the surface of a laser target, which blows off the electrons from the target and leaves positive charged ions on the surface of the target. The moving electrons create an electric field which accelerates the positively charged ions in the direction normal to the target's surface.

In the previous ICF simulation experiments, precautions as transporting the targets in an air-less environment and flushing the chamber with argon during loading were taken to prevent the lithium targets from oxidizing. However, the MTW chamber could not be flushed with argon. Consequently, an attempt was made to upgrade the film-making method to include

two different coatings on the film. In this enhancement, the lithium film layer would be covered by an additional very thin layer of tin, polyethylene, or silver. The expectation was that this additional film layer would protect the lithium from exposure to air.

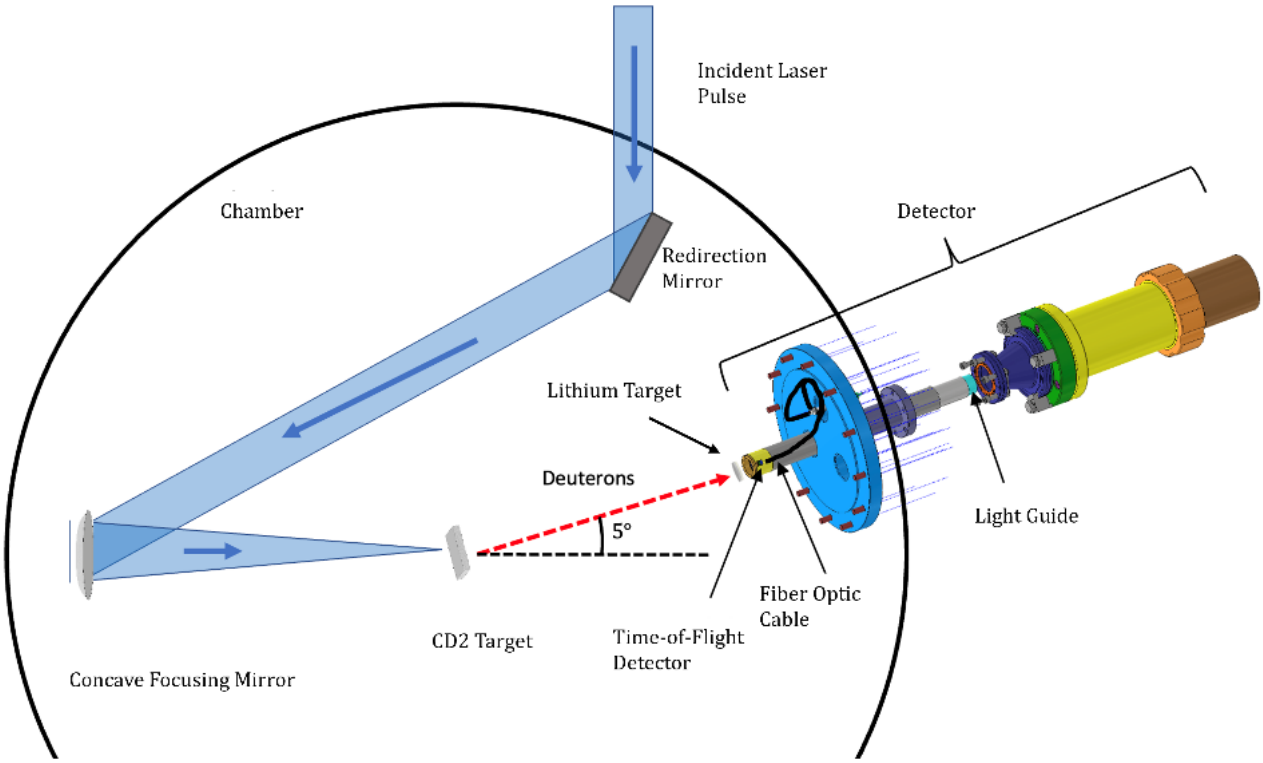

Figure 4. Overview of the experiment at MTW. The incoming laser was directed onto a CD_2 laser target, where, through the process of TNSA, deuterons were accelerated toward the lithium nuclear target which was placed just upstream of the detector to measure the decay of the reaction product.

1.2. Physical Vapor Deposition

As mentioned in the previous section, a deposition technique needed to be developed to create thin lithium films for the experiments. The desired thin lithium film would have the properties of high purity and uniformity. There are numerous film deposition methods, but Physical Vapor Deposition (PVD) was chosen as the deposition technique for this project as PVD offers the desired film properties through direct conversion of the solid material into vapor and it is a widely used method for creating thin films and coatings on substrates. There are two common means used to perform PVD: sputtering and evaporation. Both methods are

similar in that atoms are removed from the source material through physical means, and then are deposited onto the surface of the desired substrate.

The sputtering method was first discovered in 1852 by W.R. Grove during his study on the interaction between electricity with gases and liquids [3]. In this experiment he transmitted current between a steel needle and a silver plate that was separated by 0.1 inch through a medium that was a mixture of hydrogen gas and air. Then he observed the formation of a circular oxide on the silver plate as the gas between the steel needle and the silver plate was ionized. In the common process of sputtering, shown in Figure 5, a neutral gas such as Ar is injected into a chamber. Ar atoms are ionized by accelerated electrons, attracted toward the material by a potential difference. As the ions hit the target material, atoms of the target material sputter away from the surface of the target material. Then the neutral sputtered atoms flow freely and hit the surface of a substrate that is placed some distance away from the source.

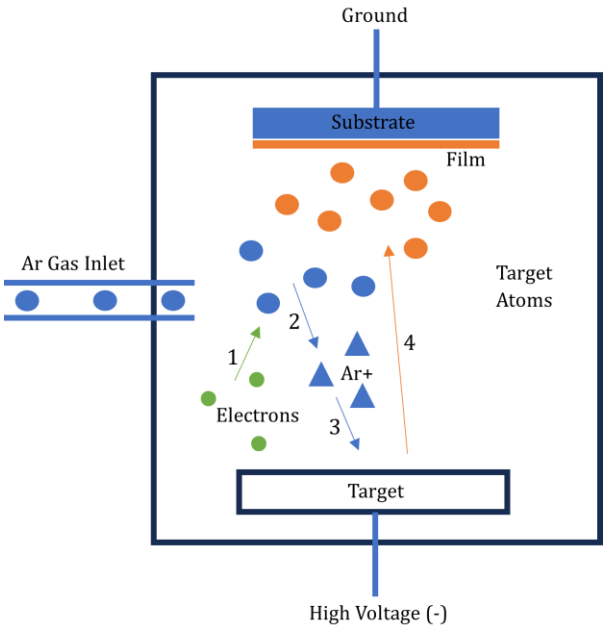

Figure 5. Overview of the sputtering process of physical deposition. Gas such as Ar is injected into the chamber. High voltage is applied between the substrate and the target existing electrons in the chamber to be accelerated. The accelerated electrons collide with Ar atoms causing them to be ionized. The positive Ar atoms hit the target causing the atoms of the target to sputter from the surface of the target and then form a layer of thin film on the surface of the substrate.

The first use of the evaporation method of PVD was conducted by Faraday in 1857 [4]. In Faraday's experiment, a gold wire was heated by a strong electric current and Faraday observed the creation of gold thin film. This observation led to the development of evaporation deposition, which is the process of using the vaporized atoms to condense and form a thin film on a substrate. The vaporized atoms can be obtained through thermally heating the material inside a vacuum to a temperature where there is an appreciable vapor pressure.

The vapor pressure is the equilibrium pressure when the rate of atoms evaporating is the same as the rate they condense on a material's solid or liquid surface at a given temperature inside a closed container. This closed container is known as the Knudsen cell, which is used to measure the vapor pressure. The dependence of vapor pressure on temperature is called the vapor pressure curve, and a higher vapor pressure will lead to a faster deposition rate. Figure 6 shows vapor pressure curves for some selected materials.

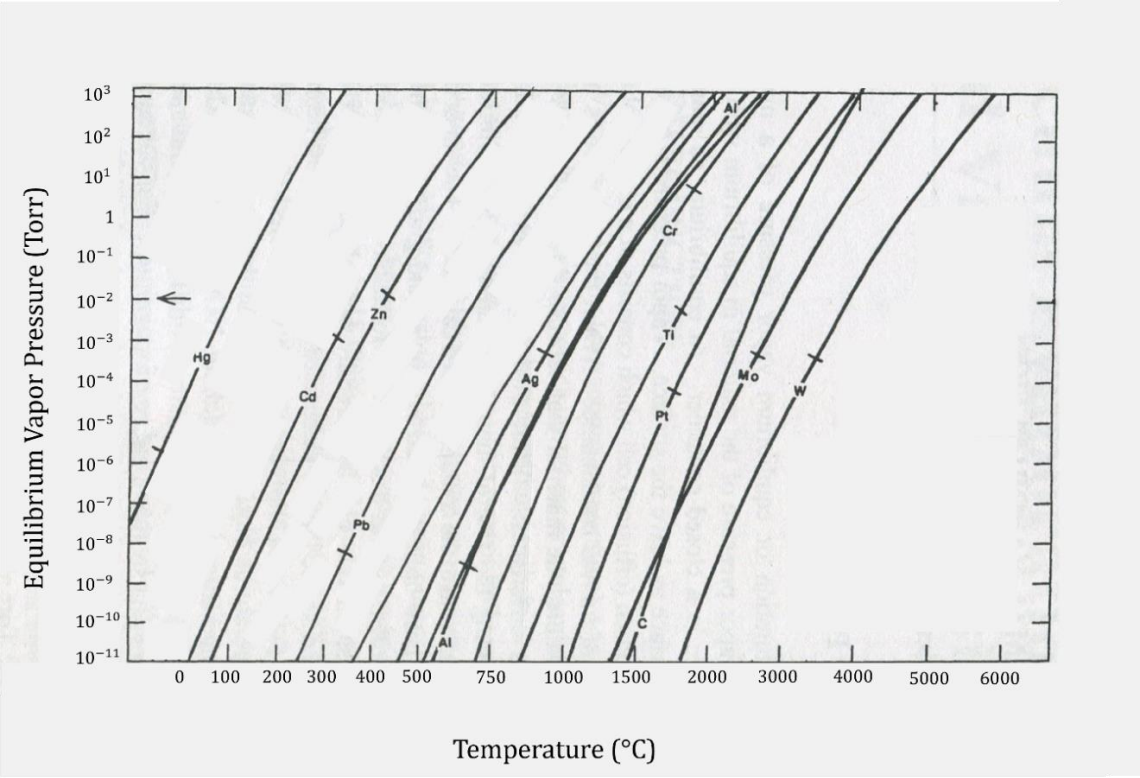

Figure 6. The vapor pressure curve for various materials as a function of temperature. Notice that for different materials at the same temperature, the equilibrium vapor pressure can be quite different. Figure taken from Ref. [5]

As shown, the equilibrium vapor pressure increases as temperature increases because the increase in temperature leads to higher average kinetic energy of the atoms which leads to higher rate of evaporation. Thus, the general process of the evaporation method is to place a desired target material in the form of solid or liquid inside of a container such as a boat or a crucible inside of a vacuum system. The container and the material inside are heated to the needed temperature which causes the material to change phase to vapor, the vaporized atoms will then hit the surface of a substate. The surface of a substrate is relatively cooler and when the vaporized atoms encounter the surface, atoms lose their thermal energy and condensed as a thin film on the substrate. The evaporation method is a continuous depositing process, the thickness depends on the deposition rate which depends on various factors such as vapor pressure, temperature, and vacuum pressure.

1.3. Evaporation Deposition at Houghton

A simplified diagram of the deposition system at Houghton is shown in Figure 7. Inside the deposition chamber, two boats are fixed horizontally on two electrodes. Two different desired target materials may be placed in separate boats inside the chamber. Each boat is connected to a diode so that the heating of each boat can be controlled by changing the direction of the flow of current through the electrodes. A container called a “house” that has an opening in the center is placed over the boats, the “house” is used to keep the evaporated atoms from sticking to other surfaces in the vacuum chamber.

The deposition process starts with pumping the chamber down to a base pressure of about 10^{-5} Torr. By using the vapor pressure curve shown in Figure 6 and the base pressure of the chamber, the temperature needed to cause a desired material to phase transform to vapor may be determined. Thus, each boat with its respective material is resistively heated by current, to achieve its appropriate temperature that creates an adequate vapor pressure. As the material starts to vaporize, the evaporated atoms will flow freely in the space contained by the house. The atoms will flow through the top opening of the house and as they hit the surface of the substrate, a thin film will start to form as the atoms condense on the surface.

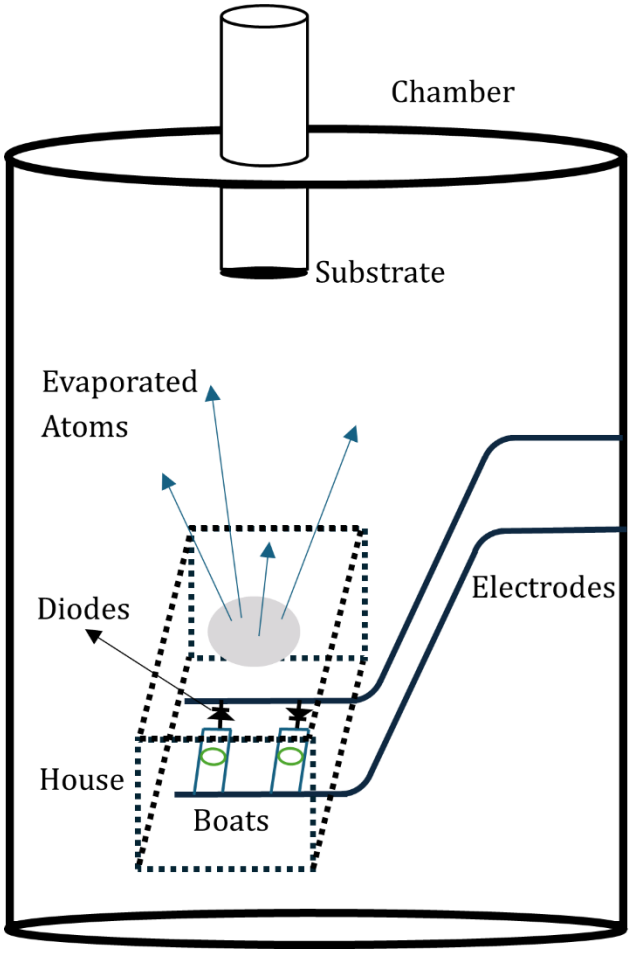

Figure 7. Simplified diagram of the deposition system. Current is applied through the electrodes to resistively heating the solid material placed inside of a boat in which the direction of the current matches with the diode. Then the material will evaporate at appropriate vapor pressure and move out from the top opening of the house. This will lead to the formation of thin film on the surface of the substrate that is held at some fixed height above.

Chapter 2

MASS DISTRIBUTION THEORY

The physical phenomenon of how the atoms of a target material are deposited as a thin film onto the substrate will be discussed in this chapter in order to predict the mass distribution of the film on the substrate. The deposition rate as a function of the position on the substrate will be derived and numerically calculated.

2.1. Mass Distribution of the Film

The experiments described in Chapter 1 used thin film targets to test the feasibility of using the SLICS detector system to study light-ion interactions, namely, by simulating an ICF implosion or using TNSA to accelerate the ions. These cross sections measurements depend on the mass distribution of the nuclear target. Thus, the predicted mass distribution of the thin film targets was calculated as described in this chapter.

To estimate the mass distribution, first imagine the target material in the boat and the substrate shown in Figure 7 are separated by some distance. During a typical evaporation deposition process, the target material is heated in a low pressure environment such that the target material starts to vaporize. As it vaporizes, the atoms of the target material travel through the evaporant surface in all directions. This phenomenon is shown in Figure 8, where evaporant surface in the boat can be divided into many infinitesimal area elements and also the surface of the substrate. Let's define the area element on the boat and the substrate by dA_e and dA_c respectively. Then the atoms leaving from area element dA_e are shooting off in all directions, and one of their many possible trajectories hits the area element dA_c.

Thus, it is crucial to consider the directional dependence of the path of the evaporant atoms in order to find the mass distribution as a function of the radius of the substrate. Figure 9 shows a closer look at the tiny area element dA_e that is in the plane of the evaporant surface, where the atoms below the evaporant surface are going in all directions and all possible velocities.

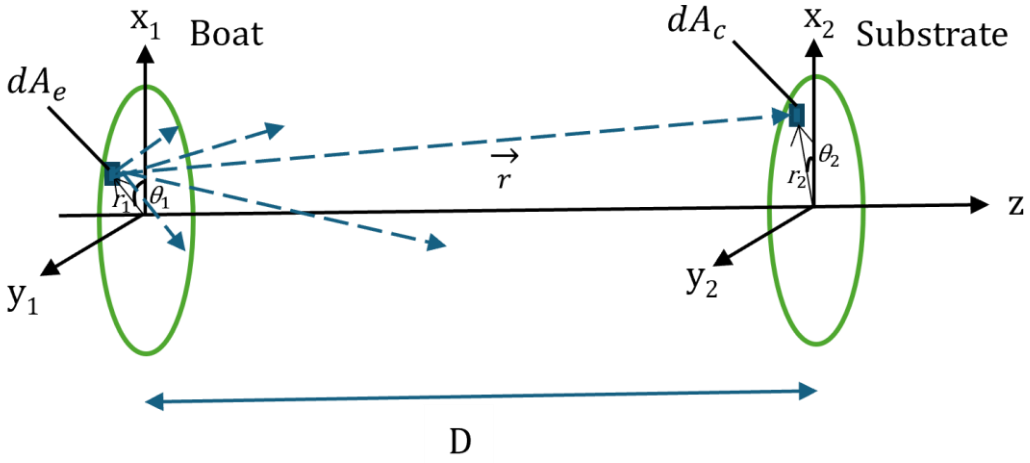

Figure 8. Atoms from boat to the substrate. In cylindrical coordinates, they are separated by distance D on the z axis, where $\vec{r}$ is the vector from the area element of the boat to the area element of the substrate. Each area element position can be described using the radius r and angle θ.

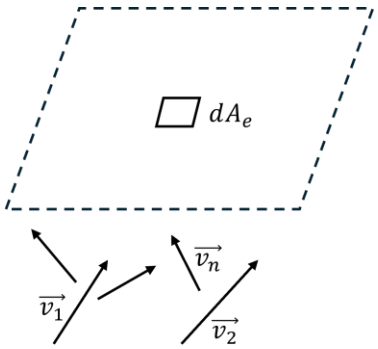

Figure 9. Overview of the heated atoms on the boat. The dashed box represents the evaporant surface and the solid box denoted by dA_e represents a small area element in the plane of the evaporant surface. The vectors below represent the velocity of atoms.

Now, assume some fraction of the evaporant atoms from the boat are traveling with velocity $\vec{v}$ with angle ϕ relative to the surface normal and are leaving the evaporant surface through the area element dA_e. All the atoms also travel through an area element denoted by dA'_e that is perpendicular to $\vec{v}$ as shown Figure 10. The small volume of atoms of evaporant travelling through dA'_e in a small time of dt can be described as,

$$dV = vdtdA'_e. \tag{1}$$

Figure 11 shows a side view of the area elements and a relationship can be made between dA_e and dA'_e,

$$dA'_e = dA_e \cos\phi, \tag{2}$$

so Equation (1) can be expressed as

$$dV = vdtdA_e \cos\phi. \tag{3}$$

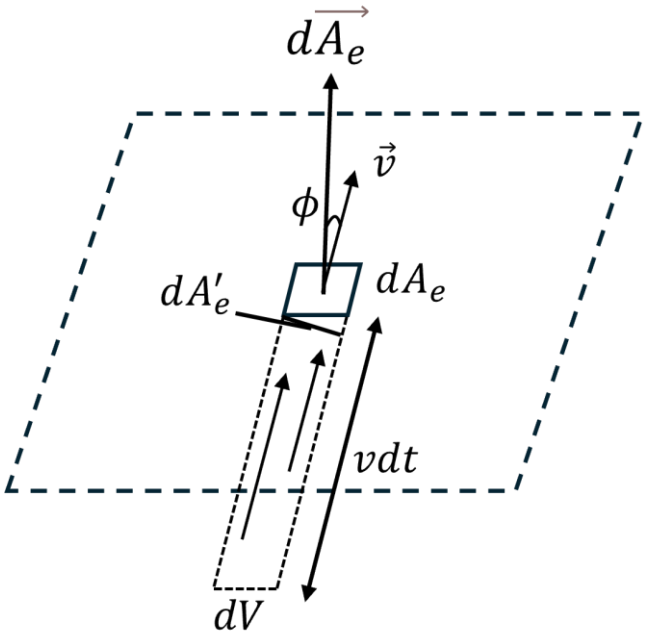

Figure 10. Overview for the movement of evaporant. The flow of the atoms of a particular velocity $\vec{v}$ and angle ϕ across the area element dA_e. Where the flow of atoms also travels across area element dA'_e which is perpendicular to $\vec{v}$. Then the volume of atoms travelling across the area elements in dt can be described.

Equation (3) describes the small volume of evaporant with a given velocity and angle travelling through the area element dA_e. As the evaporant leaves from dA_e, it is then expected to hit the condensing surface of the substrate. Similarly to the evaporant surface, the condensing surface can be divided into many small area elements, each denoted as dA_c. The atoms will hit the area elements dA_c at an angle denoted as ψ, but all the atoms will also travel across an area element that is perpendicular to $\vec{v}$ denoted as dA'_c as shown in Figure 12.

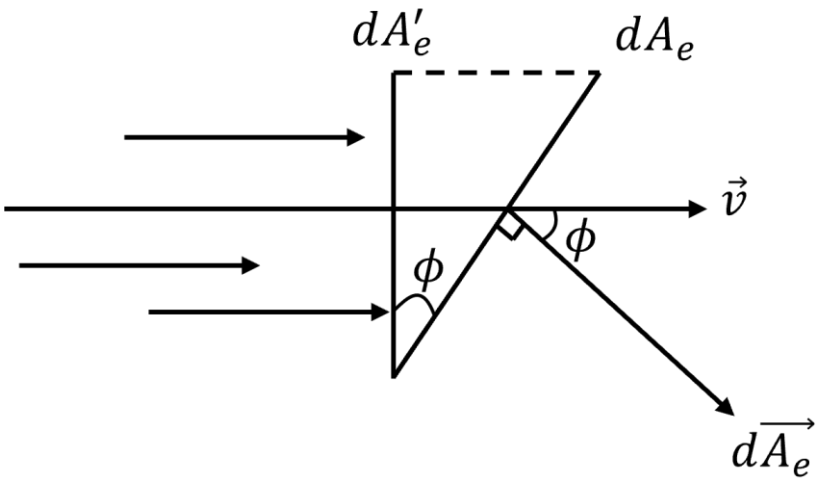

Figure 11. Overview of the angle relationship between evaporant area elements dA'_e and dA_e. The length and the width of dA'_e and dA_e are l_1, l_2, and w respectively.

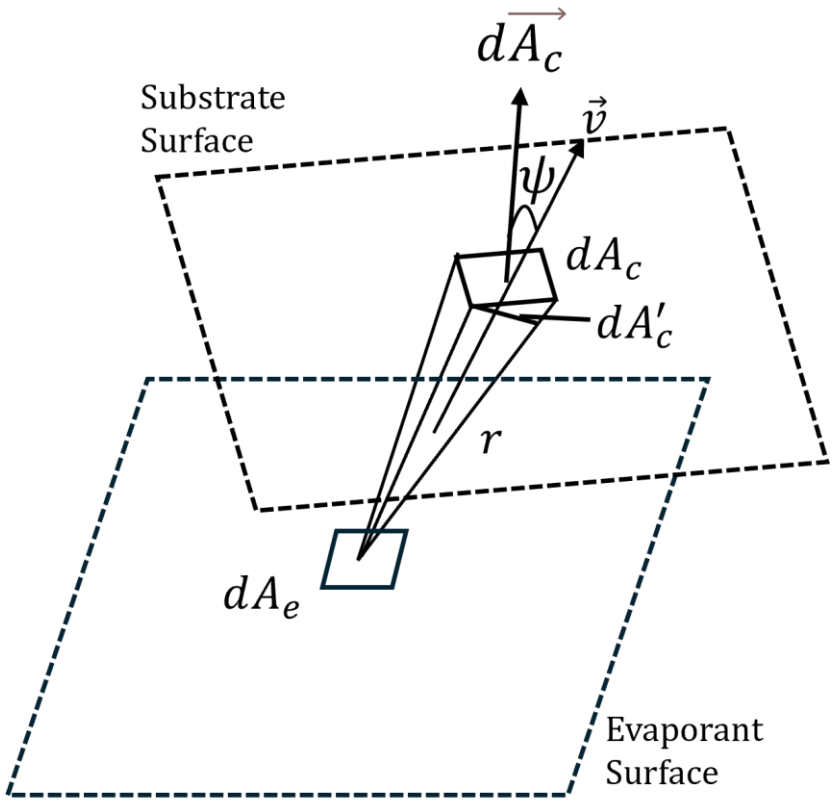

Figure 12. As atoms leave from dA_e with $\vec{v}$, the atoms will hit a small area element dA_c on the condensing surface at angle ψ relative to surface normal. All the atoms will also travel across dA'_c which is perpendicular to $\vec{v}$. The distance between the dA_e and dA'_c is r.

The solid angle $d\omega$ would be the surface area dA_c' divided by the distance,

$$d\omega = \frac{dA_c'}{r^2}. \tag{4}$$

It is important to note that the atoms coming off of dA_e travel in all directions. Thus, in order to describe the fraction f of the number of atoms going in every direction that only hit a small area element dA_c',

$$f = \frac{dA_c'}{4\pi r^2} = \frac{d\omega}{4\pi}, \tag{5}$$

but

$$dA_c' = dA_c \cos(\psi). \tag{6}$$

Thus, the solid angle equation can be rewritten as

$$d\omega = \frac{dA_c'}{r^2} = \frac{dA_c \cos(\psi)}{r^2}, \tag{7}$$

and this describes the solid angle with respect to dA_c. The number of atoms that travel from the evaporant to the substrate can be described as dN. Then the total number of evaporant atoms N times the fraction inside the volume dV which is dV/V where V is the total volume, the fractions that are going in the right direction, f:

$$dN = \frac{NdVf}{V}. \tag{8}$$

Using Equation (3), (5), and (7)

$$\frac{d^3N}{dA_e dA_c dt} = \frac{N}{V} v \cos\phi \frac{\cos\psi}{4\pi r^2}, \tag{9}$$

where $d^3N/dA_e dA_c dt$ is the rate of number of atoms leaving dA_e and condensing on dA_c, and N/V is ρ, the number density of the evaporant. In order to fully describe the number of molecules leaving from the evaporant surface element to the condensing surface element, other factors such as the sticking coefficient α_v and the probability for atoms to have the velocity between v to $v + dv$, denoted as $\Phi(v^2)dv$, need also be accounted for. The sticking

coefficient α_v is the fraction of the atoms that condense to the surface upon collision with the substrate. Thus Equation (9) becomes

$$\frac{d^4N}{dA_e dA_c dv dt} = a_v \rho v dt \cos(\phi) \frac{\cos(\psi)}{4\pi r^2} \Phi(v^2), \tag{10}$$

which represents the rate of atoms leaving dA_e and condensing on dA_c for a given velocity v. The rate of atoms of all velocities traveling from the surface element dA_e to surface element dA_c can be described

$$\frac{d^3N}{dt dA_e dA_c} = \int_0^\infty \frac{d^4N}{dt dA_e dA_c dv} dv = a_v \rho \cos(\phi) \frac{\cos(\psi)}{4\pi r^2} \int_0^\infty v\, \Phi(v^2) dv. \tag{11}$$

In order to account for the probability distribution of the atoms, $\int_0^\infty v\, \Phi(v^2) dv$, let's start with the Canonical Ensemble where the probability of finding atoms with a particular energy E is expressed as

$$P(E) = \frac{e^{-\beta E}}{Z}, \tag{12}$$

where the energy of each atom is $E = \frac{1}{2} m v^2$ and m is the mass of the evaporant atom, the partition function is

$$Z = \sum e^{-\beta E} \tag{13}$$

where $\beta = 1/k_B T$ for temperature T. Since each atom of the evaporant travels in a 3D space, the velocity $\vec{v}$ has three components (v_x, v_y, v_z). Let's start with finding the probability in one dimension v_x,

$$P(v_x) = e^{-\frac{m v_x^2}{2 k_B T}} / Z_x. \tag{14}$$

Since the velocity of each atom is continuous, integrate over all the velocities in order to account for all the possible velocities. Thus Equation (13) can be expressed

$$Z_x = \int_{-\infty}^{\infty} e^{-\frac{m v_x^2}{2 k_B T}} dv_x. \tag{15}$$

This is the partition function for one atom in one dimension. Even though Equation (15) has the limits from $-\infty$ to ∞, because of symmetry,

$$Z_x = 2\int_0^\infty e^{-\frac{mv_x^2}{2k_BT}}dv_x. \tag{16}$$

Thus,

$$Z_x = 2\int_0^\infty e^{-\frac{mv_x^2}{2k_BT}}dv_x = \sqrt{\frac{2\pi k_BT}{m}}. \tag{17}$$

Recall from earlier that Z_x only accounts for one dimension, but the partition function for the other two dimension would work the same as Z_x. Thus $Z = (Z_x)^3$ for one atom. The probability for an atom to be in the velocity of v to $v + dv$ and in all three dimensions is therefore

$$P(v)d^3v = (d^3ve^{-\frac{E}{k_BT}})/Z = \left(\frac{m}{2\pi k_BT}\right)^{3/2} e^{-\frac{mv^2}{2k_BT}}d^3v. \tag{18}$$

Since velocity has three dimensions and is between v and $v + dv$, this looks like a shell in spherical coordinates. The volume element for the spherical shells in velocity space is

$$d^3v = \int_0^{2\pi}\int_0^{\pi} v^2\sin\phi dv d\phi d\theta = 4\pi v^2 dv. \tag{19}$$

The probability of an atom having the velocity between v and $v + dv$ is therefore

$$\Phi(v^2)dv = P(v)4\pi v^2 dv. \tag{20}$$

Thus, the probability of an atom over all velocities is shown as

$$\int_0^\infty v\Phi(v^2)dv = \int_0^\infty vP(v)4\pi v^2 dv = 4\pi\left(\frac{m}{2\pi k_BT}\right)^{3/2}\int_0^\infty v^3 e^{-\frac{mv^2}{2k_BT}}dv, \tag{21}$$

where

$$4\pi\left(\frac{m}{2\pi k_BT}\right)^{3/2}\int_0^\infty v^3 e^{-\frac{mv^2}{2k_BT}}dv = 4\pi\left(\frac{m}{2\pi k_BT}\right)^{\frac{3}{2}}\left(\frac{1}{2\left(\frac{m}{2k_BT}\right)^2}\right) = \sqrt{\frac{4}{\pi}}\left(\frac{2k_BT}{m}\right)^{\frac{1}{2}}. \tag{22}$$

Then using the result from Equation (22), Equation (11) becomes

$$\frac{d^3N}{dtdA_e dA_c} = a_v \rho \cos(\phi) \frac{\cos(\psi)}{4\pi r^2} \sqrt{\frac{4}{\pi}} \left(\frac{2k_B T}{m}\right)^{\frac{1}{2}}. \tag{23}$$

Thus, knowing the rate dN/dt of molecules leaving from the surface element dA_e and reaching the condensing surface element dA_c, the rate of mass evaporation from surface A_e and condensing surface A_c is

$$\frac{dM}{dt} = \int_{A_c} \int_{A_e} m \frac{d^3N}{dtdA_e dA_c} dA_e dA_c. \tag{24}$$

Using Equation (23), it becomes

$$\frac{dM}{dt} = \int_{A_c} \int_{A_e} m \sqrt{\frac{4}{\pi}} \left(\frac{2kT}{m}\right)^{\frac{1}{2}} \alpha_v \rho \frac{\cos(\phi)\cos(\psi)}{4\pi r^2} dA_e dA_c. \tag{25}$$

Notice $\sqrt{\frac{\pi}{4}} (2mkT)^{\frac{1}{2}} \alpha_v$ is constant for Equation (25). Thus, let's denoted $\sqrt{\frac{\pi}{4}} (2mkT)^{\frac{1}{2}} \alpha_v$ as C and Equation (25) becomes

$$\frac{dM}{dt} = \int_{A_c} \int_{A_e} C\rho \frac{\cos(\phi)\cos(\psi)}{r^2} dA_e dA_c, \tag{26}$$

where $\cos(\phi) = \cos(\psi) = \hat{r} \cdot \hat{k}$ as shown in Figure 13. Moreover, $\hat{r} = \vec{r}/||\vec{r}||$ and $\vec{r}$ can be obtained by the position of the infinitesimal area element on both the boat and the substrate (x_1, y_1) and (x_2, y_2) respectively. The vector $\vec{r}$ between area dA_e on the boat and area dA_c on the substrate is the path of atoms emitted by the area element dA_e that hit area element dA_c on the substrate, which can be expressed as,

$$\vec{r} = (x_2 - x_1)\hat{\imath} + (y_2 - y_1)\hat{\jmath} + D\hat{k}. \tag{27}$$

This vector can also be expressed in terms of the coordinates in a cylindrical coordinate system. Imagine each boat in the cylindrical coordinate system as shown in Figure 14.

$$\vec{r} = (\, r_2 \cos(\theta_2) - \, r_1 \cos(\theta_1))\hat{\imath} + (r_2 \sin(\theta_2) - r_1 \sin(\theta_1))\hat{\jmath} + D\hat{k}. \tag{28}$$

Thus,

$$\hat{r} \cdot \hat{k} = \frac{D}{\sqrt{\left(\left(r_2 \cos(\theta_2) - r_1 \cos(\theta_1)\right) + \left(r_2 \sin(\theta_2) - r_1 \sin(\theta_1)\right) + D\right)}}, \tag{29}$$

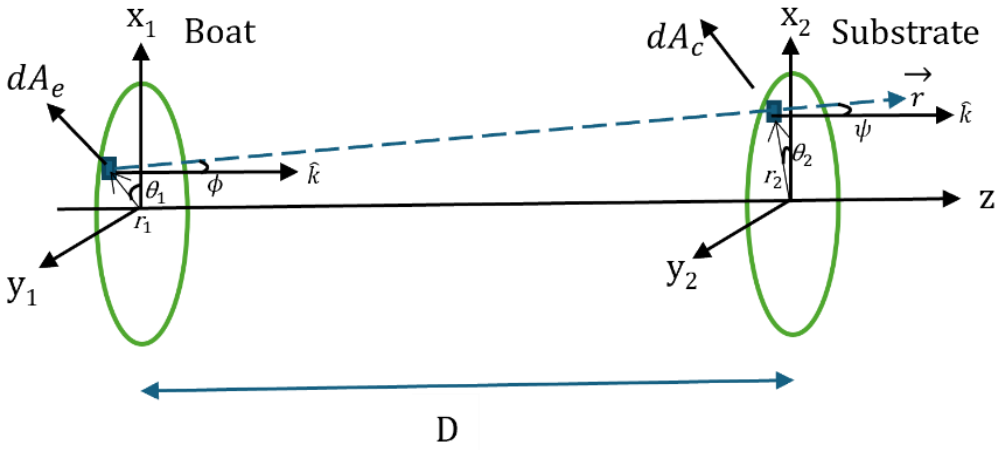

Figure 13. Similar to Figure 8 but showing the relationship between the displacement vector $\vec{r}$ and the normal vector of the surface element dA_e and dA_c.

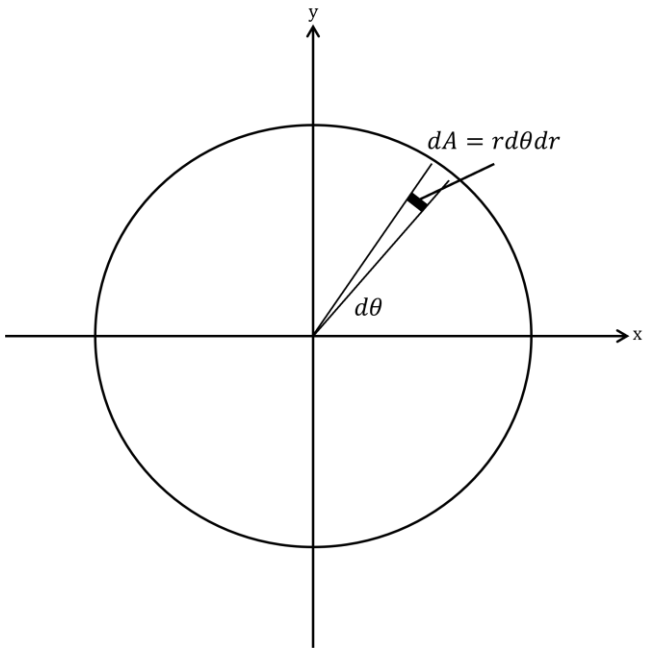

Figure 14. The evaporant in the boat in the cylindrical coordinates. An infinitesimal area element on the circle represents the small amount of a target material. The (x, y) coordinate of the area element can be described using the radius and the angle.

Then Equation (26) can be expressed as

$$\frac{dM}{dt} = \int_{A_c}\int_{A_e} C\rho \frac{\mathrm{D}^2}{r^4} dA_e dA_c = \int\int\int\int C\rho \frac{\mathrm{D}^2}{r^4} r_1 d\theta_1 r_2 d\theta_2 dr_1 dr_2. \tag{30}$$

Given the axial symmetry, the equation for mass per unit area as a function of the radius of the substrate can be obtained. This equation describes how the evaporant on the boat is depositing onto a Δr thickness ring with the radius r_2 of on the substrate as shown in Figure 15. Thus, using Equation (30) multiplied by the inverse of the area of the ring to obtain mass per unit area. However, in order to find the mass per unit area as a function of the substrate radius, dr_2 will not be integrated. Thus, the equation is described as

$$\frac{dM}{dt}(r_2) = \frac{dM_1}{dt dr_2}\Delta r \frac{1}{2\pi r_2 \Delta r} = \frac{\int_0^{2\pi}\int_0^{2\pi}\int_0^{R_1} C\rho \mathrm{D}^2 r^{-4} r_1 dr_1 d\theta_1 r_2 d\theta_2}{2\pi r_2}. \tag{31}$$

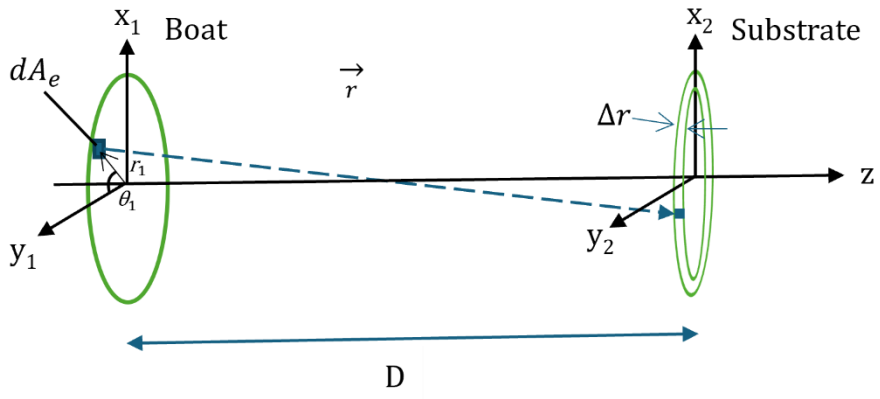

Figure 15. The evaporant in the boat depositing as a ring with the thickness of Δr on the substrate.

2.2. Numerical Integration for Mass Distribution

In Section 2.1, an integral equation was derived which can be used to describe the mass of evaporant over the condensing surface area as a function of the radius position on the condensing surface. However, the integral is not solvable analytically and must be solved numerically. Thus, numerical integration was developed to solve Equation (31) using C++ code in the ROOT analysis framework.

A program that can numerically calculate the triple integral of Equation (31) was created. The program is divided into three parts. The first part is a function called func which is shown below. This function is used to define Equation (31).

```
//Defining a function for the Triple Integral
double func(double r1, double theta1, double theta2, double r2){
   //Defining some constants in the Equation
   double M = 5;
   double rho = 5;
   double L = 3.26;
   double Rmgnitude = sqrt(r2*r2+r1*r1-2*r1*r2*(cos(theta2)*cos(theta1)+sin(theta2)*sin(theta1))+L*L);
   double result = (M*rho*r1*r2*pow(L,2))/(pow(Rmgnitude,2));
         return result;  }
```

The second part is a function called TriIntegral which calculates the total area under the curve of a given function. As shown in Equation (31), it is needed to integrate over dr_1, $d\theta_1$ and $d\theta_2$. Thus, this function takes in the lower bound for dr_1, $d\theta_1$ and $d\theta_2$, the number of steps, and the step size for r_1, θ_1, and θ_2. The lower bounds are the starting points for each of the variables. Then the number of steps of each variable are determined by the lower and upper bounds and the step size. Then three for-loops are created to loop through all the number of steps for all three of the variables that need to be integrated. Inside the loops, the value of each variable at the respective number of steps is passed into func. The values that are passed into the function func can be thought of as the dimensions of the volume element. Thus, the volume of the function for each volume element can be calculated and would be recorded. Finally, the sum of the integrated for each volume element is then returned by TriIntegral.

```
//Defining the triple Integral
//The first three terms are the low bounds, then the number of steps, and the last three terms are the step sizes of
each variables.
double TriIntegral(double lr1, double lthe1, double lthe2,
            double step, double dr1, double dthe1, double dthe2, double r2){
   //A variable that sums up the area under the function
   double Total = 0;
   //Three for loops to iterate through each varibale's step
   for(int i = 0; i < step; i++){
         for(int k = 0; k < step; k++){
            for(int z = 0; z < step; z++){
               //Finding the x value of each varibales to pass into the function to get the height of the small rectangle
               double thetai1 = lthe1+(dthe1*i)+lthe1/2;
               double thetai2 = lthe2+(dthe2*k)+lthe2/2;
               double ri1 = lr1+(dr1*z)+lr1/2;
               //Baiscally sums the area of the rectangle by having the step size times the height
```

```
            Total += ((dr1*dthe1*dthe2))*func(ri1,thetai1,thetai2,r2);
          }
        }
  }return Total;}}
```

The third part of the program is the main function which is defined as DMDTDR as shown in Appendix A. This function defines and varies things such as the lower and upper bounds of each variable. It also determines the number of steps and the step size for each variable. Arrays were created to contain the experimentally measured thickness across a sample Li nuclear target. An additional set of arrays was also created to contain the results. This function calls the TriIntegral to determine the mass over the area of the ring with the respective r_2. The experimentally measured and numerically calculated dataset were then normalized and graphed together as shown Figure 16. The black line represents the numerically calculated results which make sense that it is a straight line as there shouldn't be drastic change in mass over 0.3 cm. The curve represents three experimentally measured locations across a lithium target.

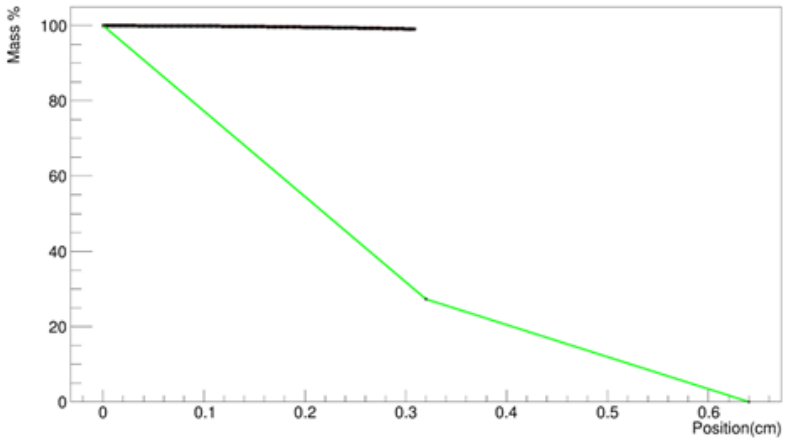

Figure 16. Graph showing the numerical and experimental values. The green line represents the experimentally measured value. The black line represents the result from the numerical integration calculations.

Chapter 3

DEPOSITION SETUP

This chapter will cover the details of each of the components that were implemented in the deposition system. There are a few major components in this system such as the physical chamber in which the deposition happened, the glove bag that was used to create an Ar environment for handling lithium, the evaporator, the power system that provided current for heating the target material, and the vacuum system that provided a low pressure environment for the deposition.

3.1. Overview of the Deposition System

The main deposition chamber and the glove bag that enclosed the chamber are shown in Figure 17. The chamber has five different ports. The top 6 inch ConFlat port was converted into a QF 40 port which gives quick access to the inside of the chamber. The port at the center is a 2.75 inch ConFlat view port that gives a side view angle. The 6 inch ConFlat bottom port has a viewport allowing a camera to observe and record the boats during the deposition process. The left 2.75 inch ConFlat port was connected to the vacuum system. Lastly, the right 6 inch ConFlat port on the right was connected to the evaporator.

Lithium was needed for making a lithium thin film and it reacts with the oxygen, nitrogen, and the water vapor in the air. Thus, a glove bag was made to enclose the chamber and create a small working space that can be flushed with Ar to remove oxygen and water vapor. A tube from the regulator on an argon pressurized cylinder was inserted into the glove bag to keep the O_2 percentage lower than 5% as measured with a Seesii 4 Gas Monitor which also monitor the humidity level inside the glove bag. The glove bag was made with 0.3 mm thick transparent polyvinyl chloride sheet as it is flexible and transparent. The glove bag was supported by a frame made of 16 mm diameter PVC pipes and 21.5 mm diameter three port PVC connectors. The length, width, and height of the glove bag is 75.5 cm, 58.5 cm, and 77.5 cm respectively. The glove bag, along with the PVC supporting frame, are placed on top of a wooden resting frame that has foam seal on the bottom to ensure a flat surface seal with the table. Additionally, two pairs of 25 inch B0819SV11W rubberized long gloves were sewed and glued with Eclectic shoe goo adhesive glue onto the top and on the right side shown in Figure 17.

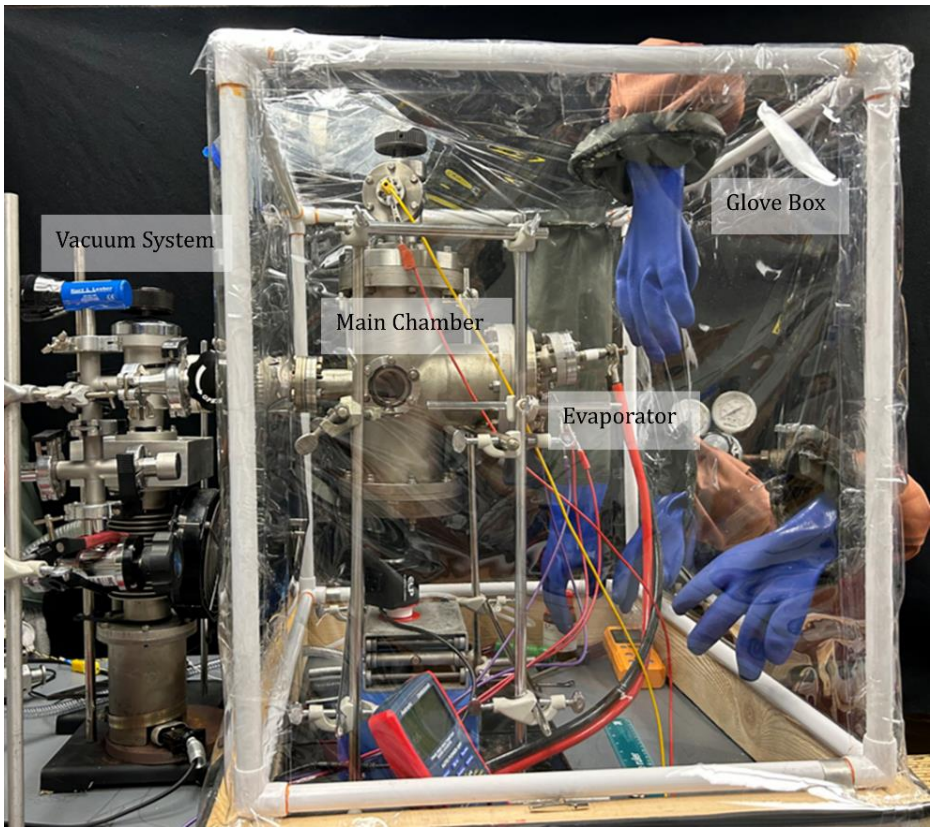

Figure 17. Sideview of the deposition system. The main chamber is in the center of the image. To the left of the it is the vacuum system. The evaporator which heats up elements of interest for deposition is inserted into the chamber from the right port. A glove bag made of transparent polyvinyl chloride sheet and PVC pipe as the framing support was constructed to create an Ar filled space to prevent Li from oxidizing.

3.2. Evaporator

The evaporator consists of various components that serve the purpose of holding, heating, and evaporating the desired evaporant to create the thin film target. All of the components of the evaporator are mounted on the electrical feedthrough Lesker EFT0523253. As discussed in Chapter 1, nuclear films with different requirements were needed for the two different experiments, so the design of the evaporator changed over time in order to satisfy the needs of the two experiments. Thus, the description of the development history of the evaporator will be separated into early and current designs.

3.2.1. Early Design

The early design of the evaporator, shown in Figure 18, produced nuclear targets for the ICF simulation experiment described in Section 1.1.1. The nuclear target for this experiment only needed a thin layer of natural Li metal on the substrate.

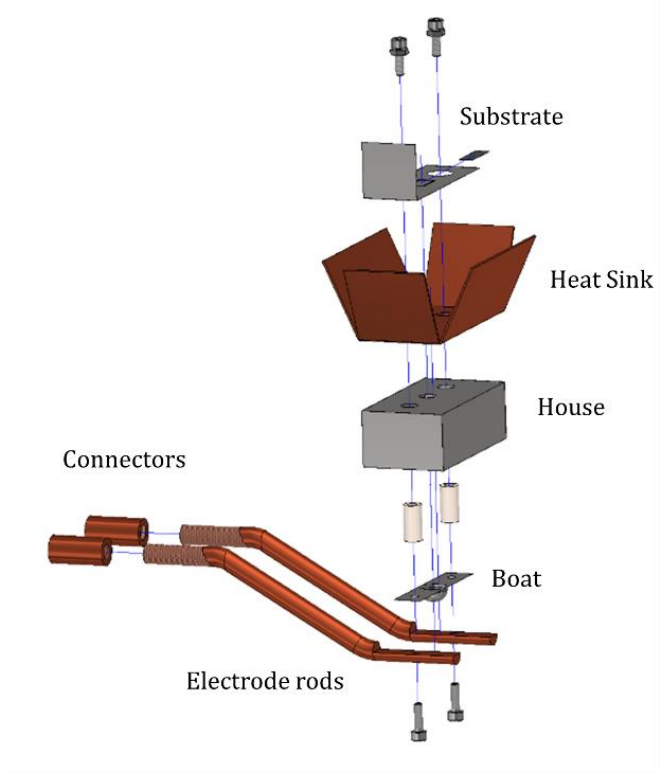

Figure 18. The exploded view of the early version of the evaporator. The copper heatsink and stainless steel house each have a hole in the middle to feed a tube onto the boat to allow it to be loaded by dropping target material through the tube. The substrate was then placed on top of the heatsink. Current was passed through the feedthrough electrodes heating boat to melt the target material. Evaporated atoms would flow upward and be deposited on the substrate though the holes.

3.2.1.1. Electrodes

Copper electrodes were attached to the feedthrough electrodes to carry current to the boat. The feedthrough has two 6.35 mm diameter, 103.7 mm long copper rods, thus, extensions were implemented to extend the rods. These extensions and connectors are detailed in Figure 18. The 6.35 mm diameter copper extensions were bent using a tubing bender. The ends of both extensions are horizontally straight where the 2 cm long upper end was threaded using ¼-28 size die to allow it to screw into the 9.6 mm diameter, 2 cm long copper connectors. The connectors were drilled using a # 3 drill bit and tapped thoroughly using ¼-

28 tapper. A ¼-28 size nut was placed between the connector and extension to ensure they are tightly and rigidly fixed. The 3 cm long lower end was milled halfway down into a flat surface, ideal for accommodating the boats directly on top of them, ensuring optimal surface contact. Moreover, a hole was drilled using # 27 drill bit in the center of the lower end.

3.2.1.2. Boat

The purpose of the 0.002 cm thick by 5 cm long by 1.5 cm wide 321 stainless steel boat is to hold the target material which is resistively heated by the current that flows through the electrodes. Two holes are drilled using a # 27 drill bit on each of the sides of the boat so it can be tightly fixed on the electrodes using 4-40 screws and nuts. A 1.25 cm radius divot was also created in the center of the boat by sandwiching the 0.002 cm stainless steel sheet between two wooden boards and a 1.25 cm diameter ball bearing. Thus, the target material can be placed securely inside the divot without falling out of the boat.

3.2.1.3. House

As shown in Figure 18, the 0.002 mm thick by 6 cm long by 3 cm wide by 2 cm high 321 stainless steel "house" is placed above the boat on 3.5 mm diameter by 12.7 mm height ceramic spacers using M3 x 8 screw and an M3 nut. The ceramic spacers are fixed on the same screws that were used to fix the boat on the electrodes. The purpose of the ceramic spacers was to electrically isolate the house from the current flowing through the electrodes. The house was used to cover the boat so it can contain as many evaporated Li atoms as possible while minimizing the amount of lithium that sticks to the chamber wall. The three holes on top of the house were made with a size B drill bit. The hole at each side is 1.75 cm from the adjacent side of the house and is used to fix the house with the ceramic spears. The 6.05 mm diameter hole in the middle is 3 cm from either adjacent side and is used for multiple purposes such as the feedthrough for the natural lithium pellets onto the boat and an opening for the evaporated Li atoms to travel to the substrate.

3.2.1.4. Heat Sink

In this early design, the substrate was placed on top of the house in such a way that it faced and blocked the opening that the evaporated Li atoms traveled through. The thermal radiation from the heated boat also struck the substrate. It was not desired for the substrate

to heat up as this would interfere with the formation of film on the substrate because the evaporated atoms may not condense on the substrate and the condensed atoms may vaporize again. Thus, a 0.7 mm thick by 6 cm long by 3 cm copper heat sink was placed between the house and the substrate as shown in Figure 18. The 6 cm long by 3 cm wide flaps and the 3.6 cm long by 3 cm wide short flaps dissipated heat away from the substrate. This heat sink also has three holes and the holes serve the same purposes and have the same dimensions as the ones in the house.

3.2.1.5. Thermocouples

It is crucial to heat the boat and the lithium to the appropriate temperature. Also, it is desirable to know the temperature of the substrate, to ensure that the substrate is not overheating and affecting the formation of the thin film. Thermocouples were attached to the backside of the divot of the boat and the center opening of the heat sink which is in close proximity to the substrate using Rutland Products Furnace Cement which can withstand 2000 F once the cement has cured. Thermocouples were made by spot welding Chromel and Alumel wires together using a SUNSTONE CD320DPM2 spot welder. The combination of the wires was then connected to two 1.33-inch conflat thermocouple feedthroughs.

3.2.2. Current Design

The current design of the evaporator shown in Figure 19 was developed for making nuclear targets for the TNSA experiment. This new experiment required muti-layered thin films. In order to produce multi-layered target, two boats were used so different materials could be deposited on the same substrate. One boat is the stainless steel boat described in Section 3.2.1.2. and is used for Li deposition. The second one is a Lesker EVSME7005MO 0.122 mm thick by 47.62 cm long by 7.14 cm wide Molybdenum boat with a 4.76 mm diameter divot. It was used for other materials such as Sn, Ag, or polyethylene.

The extension rods were also redesigned so two boats could be fixed on the flat surface of the rods. The 3.8 cm long lower end was flushed halfway down into a flat surface, and three holes were drilled using # 27 drill bit in the lower end. The hole on each side is 0.75 cm away from its adjacent side. The side of the boat without the diodes was fixed onto the extension rod through M3 x 8 screws and size M3 nuts. The side of the boat with the diodes was fixed

onto the extension rod but electrically isolated by using M3 x 16 ceramic screws and size M3 nuts. The hole in the center of the flat surface was used to support the new designed house using M3 x 35 screws, M3 nuts, and 3.5 mm diameter by 12.7 mm height ceramic spacers.

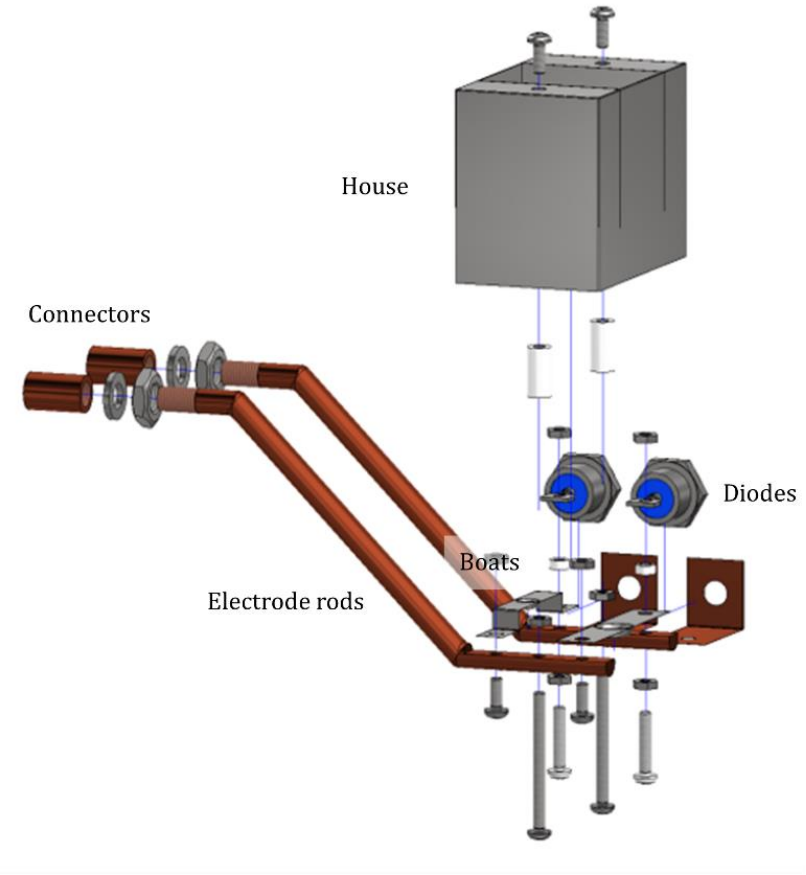

Figure 19. Exploded CAD drawing of the current design of the evaporator. Current passes through the electrodes heats up one boat at a time using diodes.

The updated "house" still served the same purposes as the earlier version, but the dimensions and the opening of the "house" were changed as the dimensions of the electrode and size of the thin film also changed. The 6 cm long by 3.8 cm wide by 4.9 cm high new "house" used 321 stainless steel. The hole on each of the sides was produced in the same fashion and served the purpose as before. The 3.8 cm long by 3 cm wide opening in the center of the house was created to ensure the maximum possible uniform coating of films on the substrate as the substrate was held at 6 cm above the center of the house.

3.2.2.1. Diodes

The updated evaporator could deposit two layers of different materials on the same substrate. It was important to only heat one boat at a time because heating up both boats would create a thin film that was a mixture of both materials. 70HFR120 and 70HF120 diodes allowed current to flow through one boat at a time as shown in Figure 20. These diodes can withstand a forward current bias of 70 A.

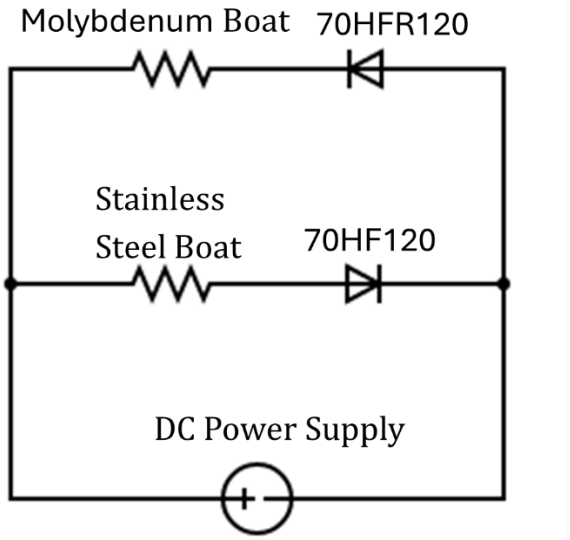

Figure 20. Schematic of the circuit for the boat, diodes, and the power supply. The diodes used were 70HFR120 and 70HF120.

3.3. Power System

A 50 A Mastech HY 1550EX and a 60 A CicuitSpecialist CSI-1560 were used to provide the appropriate current needed for deposition. A pair of 10 mm thick electrical cables was used to connect the cathode and anode of the power supply to the external leads of the electrical feedthrough. The direction of the current can be reversed by reversing the electrical cables that were connected to the electrical feedthrough.

3.4. Vacuum System

The vacuum system is an important part for the evaporation method of PVD as it creates a clean environment and low base pressure for deposition. Figure 21 shows the schematic diagram for the vacuum system. This setup allows the chamber to be opened up to atmosphere pressure while keeping the diffusion pump evacuated. This is needed for

different phases of the film production. As the first step, the chamber was be pumped down to 20 mTorr using Varian PTSO3001UN1V forepump.

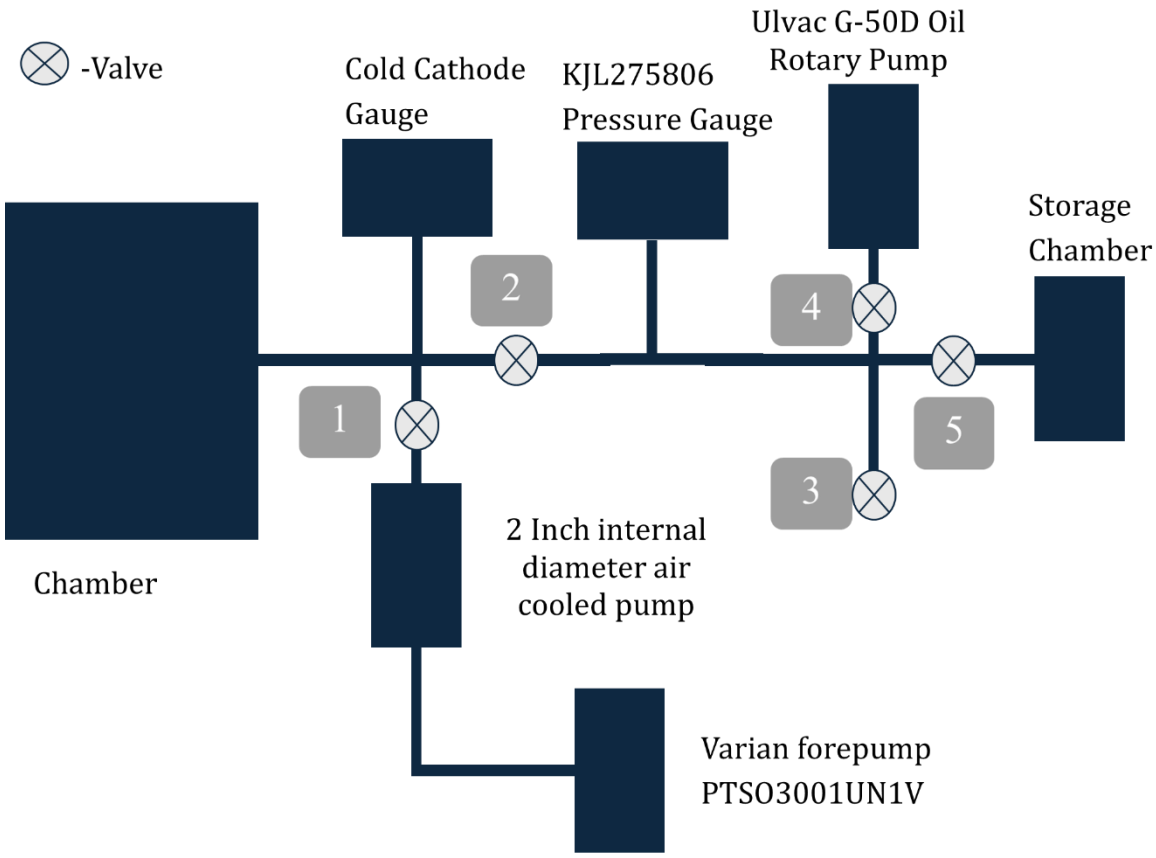

Figure 21. Schematic diagram of the vacuum system. This setup allows the chamber to be brought up to atmospheric pressure for different phases of the film production while keeping 10^{-5} Torr in components behind valve 1. Then using Ulvac G-50D oil forepump, the whole system except the components behind valve 1 can be pumped down to 20 mTorr, which satisfied the needed operating pressure for letting the 2 inch Internal diameter air cooled pump begin pumping on the whole system.

Then the 2 Inch internal diameter air cooled diffusion pump evacuated the whole set up to 10^{-5} Torr while having valve 3 and 4 closed. Valves 1 and 2 were closed before the chamber itself was brought up to atmospheric pressure using argon so the Li or any other materials or the target film were loaded into or removed from the chamber. Thus, components behind valve 1 would stay at 10^{-5} Torr during the time when the main chamber was at atmospheric pressure. Then valves 2 and 4 would be opened, allowing the Ulvac G-50D oil rotary forepump to bring the chamber to 20 mTorr. Then valve 1 were opened slowly right after

closing valve 4, causing the pressure inside the chamber to quickly reach to 10^{-5} Torr and this quick process of bringing the chamber down to desired pressure led to faster production processes.

Additionally, a separate small storage chamber was built using a 2.75-inch conflat “tee” to keep the thin Li films from oxidizing. The storage chamber pressure was kept low by having valve 5 opened when the rest of the system was at low pressure. The storage chamber also served to transport the Li films to the accelerator at SUNY Geneseo and it was able to keep a base pressure around 100 mTorr.

Chapter 4

DEPOSITION PROCESS AND TARGET RESULTS

The various components such as the main chamber, the glove bag, the evaporator, the power supply, and the vacuum system of the deposition system were described in detail in the previous chapter. The procedure for using each component of the deposition system to produce thin film targets will be described in this chapter. The resulting lithium film targets will be described and analyzed in this chapter.

4.1. Pure Natural Lithium Film Production

4.1.1. Procedures

The process of creating a lithium film began with removing the air and moisture inside the chamber using the vacuum system. The chamber was pumped down to around 20 mTorr by the Varian PTSO3001UN1V forepump, then further reduced to around 5×10^{-5} Torr by the 2-inch internal diameter air-cooled diffusion pump. Next, approximately 0.04 g of Li metal pellets were prepared and weighed inside the glove bag, which had been flushed with Ar until the O_2 percentage below 5% and humidity below 20% as measured with a Seesii 4 Gas Monitor. Argon was chosen because Li metal is stable in an Ar environment [6]. The main chamber was then brought up to atmospheric pressure using Ar, after which the Li metal pellets were loaded onto the divot of the stainless steel boat through a 6 mm diameter aluminum tube.

Once all Li pellets were loaded onto the boat, the substrate was placed in a stainless steel holder on top of the heat sink inside the chamber. Then, the chamber was pumped down to around 20 mTorr by the Ulvac G-50D oil rotary forepump and brought down to 5×10^{-5} Torr by opening valve 1 in Figure 21. Around 15 A from the Mastech HY 1550EX power supply was passed through the boat to heat it to about 470°C as measured by a thermocouple attached to the boat. As the temperature of the boat started to rise, it began to glow in a white color, progressively becoming brighter with the temperature increase. Although the actual color of the boat was orange, the SVPRO 1080P HD optical zoom camera used to capture these images had its own color filter. Shortly after the temperature of the boat surpassed

180°C, the Li pellets began to melt, visually observable as a dark spot, as shown in Figure 22 (left). This dark spot emerged because the temperature of the melted lithium was cooler than the temperature of the other parts of the boat due to the phase transformation. As the melted lithium continued to evaporate over time, the dark spot gradually decreased in size, as depicted in Figure 22 (middle). Eventually, all the lithium evaporated completely, and the dark spot faded away entirely, indicating that all the lithium had been evaporated, as seen in Figure 22 (right). Once all the Li had evaporated, the power supply was turned off and then the chamber was brought back up to atmospheric pressure using Ar. The Li film on the holder was then extracted from the chamber using a tweezer, was photographed, and its thickness measured using micrometer. It was then stored inside the storage chamber that was kept at 20 mTorr to prevent oxidation. The films were transported in the storage chamber to the experiment site at a pressure under 200 mTorr.

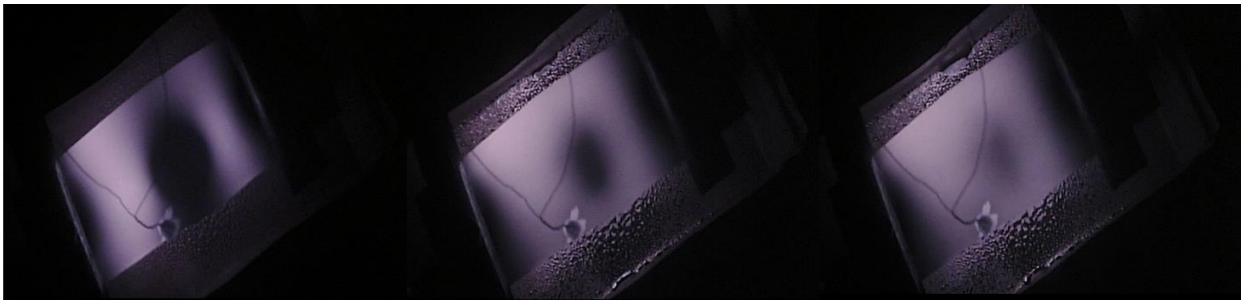

Figure 22. Evaporation process of Lithium. As the lithium melted, it formed a cool dark spot on the boat (left). The boat temperature stayed near 400 °C, as the diameter of the dark spot slowly decreased (center). Once the area of the dark spot faded completely, the lithium was all evaporated (right).

4.1.2. Results

Many Li films were produced for the ICF stimulation experiment. Figure 23 shows several of the Li films deposited onto 5 mm by 16 mm tungsten substrates. These samples also illustrate the oxidation process over time. The top left image shows a typical goldish looking lithium film right out of the chamber. The top right image displays an oxidized film after removal from the chamber but that was kept inside the glove bag for about 5 min. The bottom left image is oxidized film that was exposed to air for about 2 min, with the compound on this film believed to be a combination of lithium hydroxide and nitride due to its black color

coating. Lastly, the fourth image depicts another oxidized film that was exposed to air for 10 more minutes than the previous sample, with the white color indicating it was lithium oxide.

Figure 23. Image of lithium sample targets. (Top Left) This was used for the ICF stimulation experiment as it was not exposed to air in comparison to the other samples shown here. The lithium compound in this sample remains unknown. (Top Right) A sample that had a light grey appearance right out of the chamber. (Lower Left) A sample that was exposed to air right out of the chamber. It quickly turned from the color shown in top left to this dark color as it reacted with the air to form a black coating of lithium hydroxide and nitride. (Lower Right) This was a sample that got exposed to air for a much longer period of time. It turned from the black shown in lower left to white which is the color of lithium oxide. The thickness of these samples was measured using a micrometer and were 43 μm, unknown, 52 μm, and 23 μm respectively.

4.2. Natural Lithium Film with an Additional Coating

4.2.1. Procedures

As the deposition system was redesigned to enable the production of multi-layered targets, the procedures also changed. The new deposition process began by pumping the chamber down to 5×10^{-5} Torr for similar reasons as before. Then, the chamber was brought up to air to load the Li metal pellets into the stainless steel boat and either Sn, Ag, or polyethylene pellets into the molybdenum boat. The substrate was attached to the flat surface of the rod using three flaps from a stainless steel ring on the rod. The rod was screwed onto a linear motion feedthrough, and together were inserted into the chamber so that the substrate was placed above the boat with ability to adjust height. Subsequently, the chamber was brought down to 5×10^{-5}Torr in a similar fashion as before.

Next, 10 mm diameter electrical cables from the power supply were connected to the electrical feedthrough in such a way that the current would flow only through the diode connected to the stainless steel boat. Similarly, 15 A passed through the stainless steel boat until all lithium evaporated, which was observable through using camera underneath the chamber. Then, the electrical cables were reversed so that the current direction would also be reversed, flowing only through the molybdenum boat. In this configuration, 54 A was passed to heat up the Sn pellet on the molybdenum boat to about 1100°C, 30 A was passed to heat up polyethylene pellets to 400°C, or 50 A to heat up the Ag pellet to 800 °C.

4.2.2. Results

All of the films were deposited onto 1 inch diameter by 0.002 inch grade 321 stainless steel substrate. Each material such as Sn, Ag, or polyethylene was deposited on top of the Li layer to test if the additional layer would solve the lithium oxidization issue. Unfortunately, the additional layer made of Sn, Ag, or polyethylene did not stop the oxidization once the Li targets were exposed to air as shown in Figure 24. A particular oxidization phenomenon was observed with the polyethylene coated lithium film as polyethylene is a transparent coating, that the oxidization of lithium started from the edge the film. This indicated that the edge of the Li film was not protected from air as the diameter of the second coating was not larger than the first coating such that it did not enclose the first coating. Other factors such as the uniformity, cross-contamination, and the temperature of the substrate are also being considered as potential contributors to the failure of the additional layer in preventing Li layer oxidation.

The issue of uniformity was a result of the substrate not being aligned with the center of either boat, as the substrate was aligned with the center of the house which was between the boats. Consequently, the thin film of each layer on the substrate formed a gradient coating instead of a uniform one. Moreover, the stainless steel boat and the molybdenum boat were exposed to each other, allowing evaporated Li atoms from the stainless steel boat to possibly deposit onto the molybdenum boat used for depositing Sn, Ag, or polyethylene. This may have led to cross-contamination, potentially resulting in alloy formation on the substrate, which may have also contributed to oxidation. The suspicion of an alloy forming on the

substrate was raised by the results of Rutherford Backscattering (RBS) which was done as one of the methods for measuring the thickness of the films. RBS did not indicate sharp boundaries between layers of lithium and tin. More details for thickness measurement methods will be discussed in the next chapter.

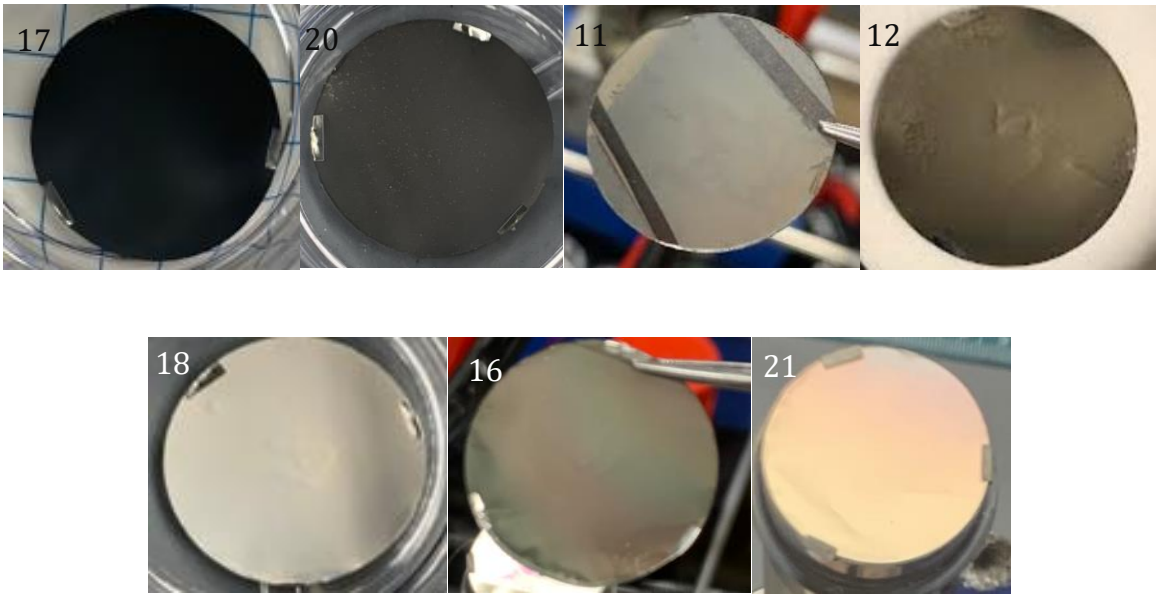

Figure 24. Image of coated and uncoated lithium targets. Target 17 was an uncoated 13.7 μm Li target shortly after removal from the chamber. Target 20 was an uncoated 9 μm Li target after a longer exposure to air such that lithium hydroxide formed. Target 11 was a 3.7 μm tin-coated Li target with two uncoated strips used for thickness measurements. Target 12 was a 6.7 μm tin coating on the lithium film. Target 18 was an 8.3 μm target that shows white lithium oxide formed under a waxy polyethylene coating after prolonged air exposure. Target 16 was another polyethylene-coated Li target with unknown thickness, where lithium oxide was forming near the edge where air is getting under the coating. Target 21 was a silver-coated lithium film with unknown thickness.

Chapter 5

THICKNESS ANALYSIS

Besides the composition and layer structure of each of the targets, another important piece of information about the targets would be the thickness. By knowing the thickness of each film, the relationship between the thickness and other factors that impact the thickness such as the weight of pellets and the distance between the substrate and the boat may be understood.

Through a better understanding of the relationship between the weight of the lihtium and thickness, desired thin thickness film may be produced by completely depositing the appropriate weight of lithium. This is desirable because the film thickness has an impact on the energy spectrum of the incident particles when performing activation experiments such as the ICF stimulation and TNSA experiment. If the incident particles hit a thick film target, the energy of the incident particles would change from monoenergetic to a wide range of energies as particles los energy when travelling through the thick film. Since the cross section is dependent on the energy of the incident particles, this would lead to difficulties for the cross section analysis as the incident particles would no longer be monoenergetic. Moreover, knowing the thickness of each film leads to a better understanding of the areal density of the nuclei on each target, which is important for calculating the number of product nuclei created, which is essential for cross section calculations.

Due to the nature of the targets being conductive coatings (lithium metal or tin-coated) on conductive, but non-magnetic stainless steel substrate, few thickness measurement methods are useable. However, a Mechanical Micrometer, a Magnetic Adhesion Tester, Rutherford Backscattering, and Profilometer were tested for their ability to measure the thickness of these targets.

5.1. Mechanical Micrometer

A Mitutoyo IP54 mechanical micrometer was used to measure the thickness of the targets. The micrometer has an original large circular surface that clamps on the film for measuring

the thickness. Since the films did not have uniform coatings and the area of the film was smaller than the diameter of the circular surface, the large circular surface measured the highest thickness point on the film surface that was enclosed by the micrometer. However, a smaller circular tip that could measure points across the film resulted in more localized reading. This is because the thickness measurement of a point on the film was not affected by the thickness of nearby points. Figure 25 shows a comparison measurement between these two tips conducted at various locations on a sample target. As observed, the small tip was able to give sharper readings of the thickness across a sample lithium film where the original tip's reading was affected by other locations on the film.

This tool was easy to use for measuring the thickness but there are two major disadvantages. First, the tip of the micrometer often caused scratches on the film. Second, the micrometer has can not measure the thickness of the individual layers.

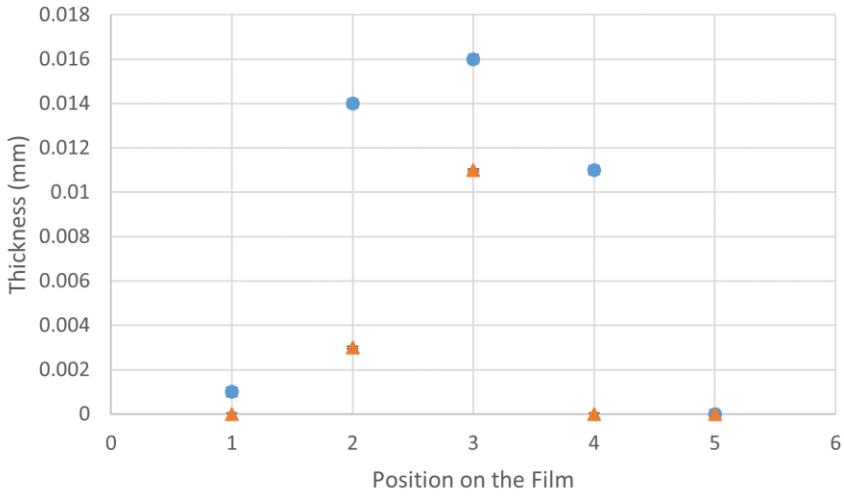

Figure 25. Lithium target micrometer thickness measurements by different sized tips across a Li target at various locations. The circular points correspond to the original large circular tip measurements and the triangle points correspond to the measurements done using the smaller circular tip. The thickness of the substrate was subtracted from all these measurements as the thickness of the substrate was measured prior to the deposition process.

5.2. Magnetic Adhesion Tester

A Magnetic Adhesion Tester (MAT) measures the thickness of a film by assessing the adhesion force between the magnetic probe of the tester and the magnetic substrate [7].

Thus, the thickness of the film between the probe and the substrate affects the adhesion force, and the tester can determine the thickness based on the adhesion force using previous calibrations. A limitation of this method is that the substrate must be magnetic, and the film must be non-magnetic.

A Neoteck NTK 103 thickness gauge was utilized to measure tin-coated lithium film deposited on 0.5 mm thick type magnetic steel substrates. The gauge was calibrated using thin plastic films before measuring the targets. Subsequently, the thickness of the targets was determined by pressing the probe of the gauge perpendicular to the surface of the targets. It was observed that the gauge was highly sensitive to the angle of the probe when making contact with the targets, posing a challenge as the thickness measurements varied significantly with different placements of the probe. There was limited data collected using MAT, since most films were deposited on non- magnetic stainless steel substrates. Moreover, the probe was sharp and often scratched the film itself during placement as shown Figure 26.

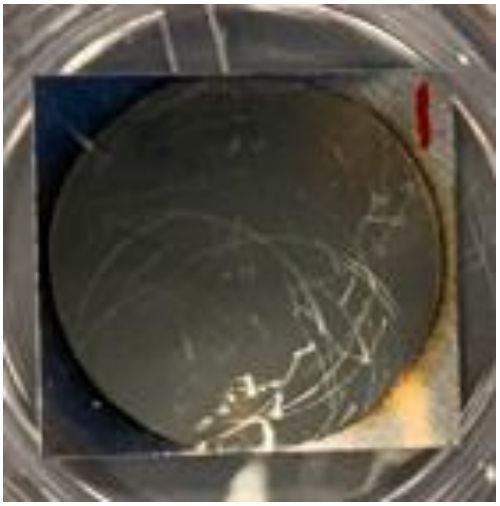

Figure 26. The scratches were made by the MAT on a lithium target.

5.3. Rutherford Backscattering

Rutherford Backscattering (RBS) is a well-known method for measuring the thickness of thin films. This thickness measurement technique was carried out using the Pelletron Accelerator at SUNY Geneseo. Approximately 2 MeV proton particles beam was directed onto the nuclear

target such that $^{7}\mathrm{Li}(\mathrm{p},\alpha)^{4}\mathrm{He}$ occur, and a silicon detector was placed at backward angle to measure the alpha particles as shown in Figure 27.

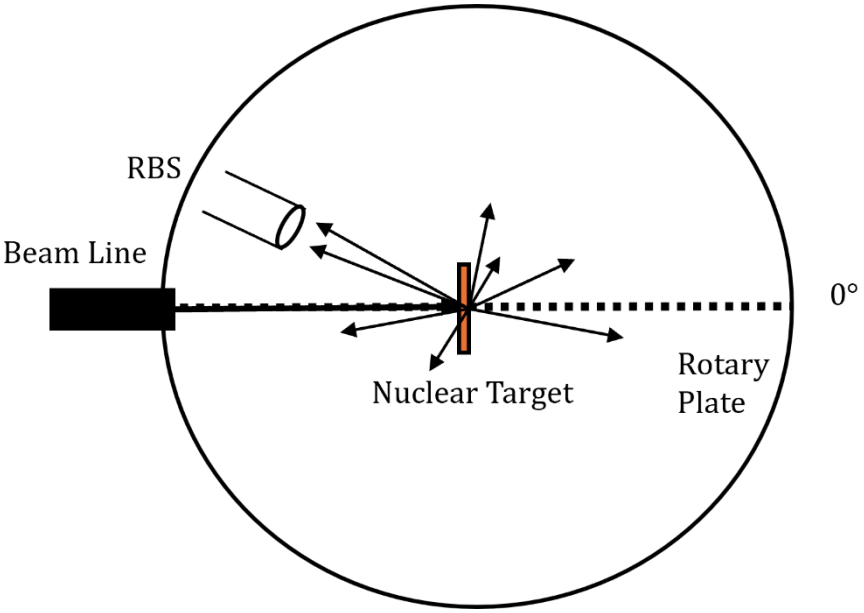

Figure 27. Diagram showing the RBS setup. Incoming protons strike the nuclear target. The protons elastically scattered backward were detected by the RBS detector.

Then the thickness of each composition layer on the target was determined by analyzing the measured spectrum. The size and shape of the peaks on the spectrum were fitted with theoretical model to determine the thickness of a particular component on the target.

RBS worked well for determining the thicknesses of the target layer with known composition, but it was difficult for some oxidized lithium targets that contained unknown compounds. However, even though it was difficult to determine the density, the areal density of each isotope could be measured. Figure 28 shows the areal density measured by both RBS and micrometer for the same targets. The dash line represents $y = x$ where the dotted line is represents the linear fit and notice that micrometer thickness value is always greater than the RBS thickness value. This makes sense because the micrometer's measurements would take into account of all the lithium compounds on the film where RBS measures the thickness of just lithium.

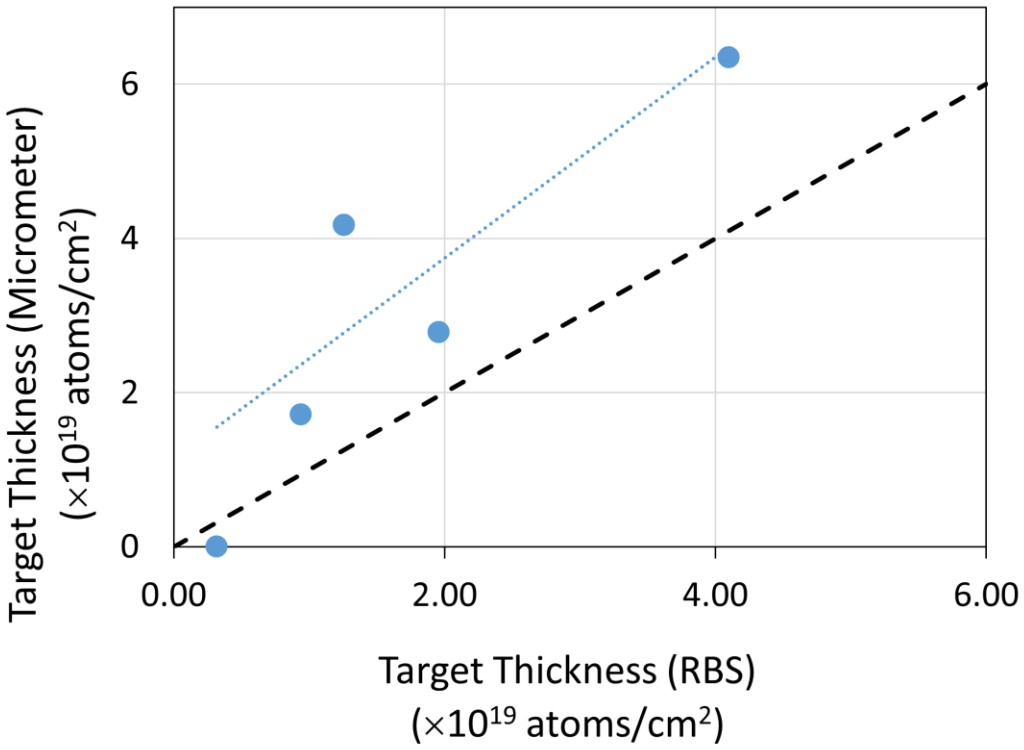

Figure 28. RBS and micrometer areal density data comparison. The dash line represents what would look like if RBS and micrometer agree on the areal density. The dotted line shows a linear relationship such that the areal density measured by micrometer is always thicker than RBS as micrometer includes the areal density of various oxidized lithium compounds.

5.4. Profilometer

The last method used for measuring the thickness was a home-made profilometer. This profilometer consisted of three parts as shown in the schematic diagram in Figure 29. The first component was the Yeebyee 150 mm Linear Rail Guide powered by the NEMA17 Stepper Motor. The target was fixed onto a grounded platform that was attached to the rail. The second component was the New Focus 8302 Picomotor Pizeo Linear Actuator which used piezo crystals to turn a finely threaded rod in tiny increments to move the probe in steps of about 10 nm. The last component was the Vernier Rotary Motion Sensor which measured the rotation of the threaded rod by the picomotor to determine the linear distance. All these components were controlled by the Raspberry Pi 4 Model B using a program in Python as shown in Appendix B. The program was created by Dr Yuly.

Thus, using this setup, a profile of target thickness could be scanned. The target was fixed onto the rail guide. The picomotor powered the probe to move in the x-axis in steps of approximately 10 nm until the tip of the probe touched the surface of the target, which resulted in an electrical connection as the target was grounded. Then the distance it took for the probe to touch the surface of the target would be recorded and the probe would back out some fixed distance. The stepper motor would move the target in the y-axis. These steps continued until it had scanned across the entire surface of the target.

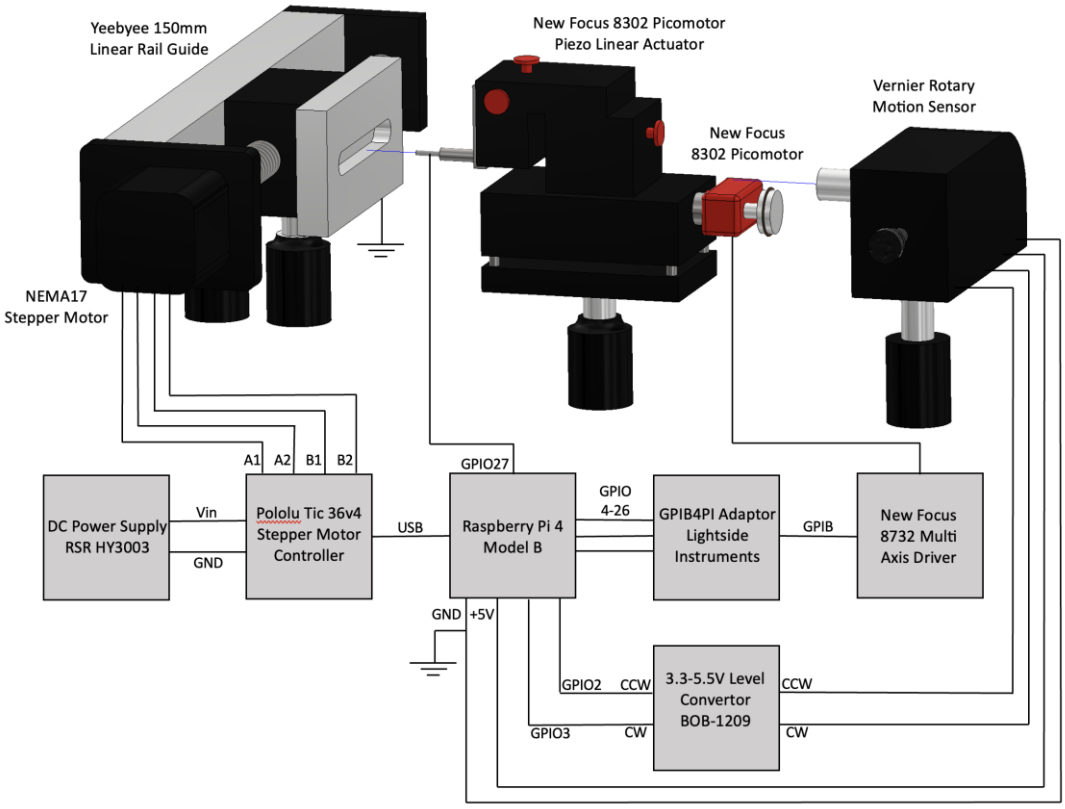

Figure 29. Schematic of the Profilometer. Target was fixed onto the Yeebyee 150 mm Linear Rail Guide, allowing the whole surface of the targets to be scanned. Targets on the rail guide were grounded. The New Focus picometer used piezo crystals to turn a finely threaded rod to move the probe in steps of about 10 nm. As the probe came in contact with the surface of target, electrical connection was made causing the rotary encoder to capture the absolute position.

Figure 30 shows two calibration profiles obtained by scanning across a well-polished steel gauge block (left) and scanning across a 15.2 μm thick aluminum foil strip and a 25.4 μm thick stainless-steel foil strip on a substrate (right). The profilometer was able to distinguish

the peak of each strip on the substrate. The inconsistent data points are believed to be caused by the fact that the strips were not perfectly flat on the substrate.

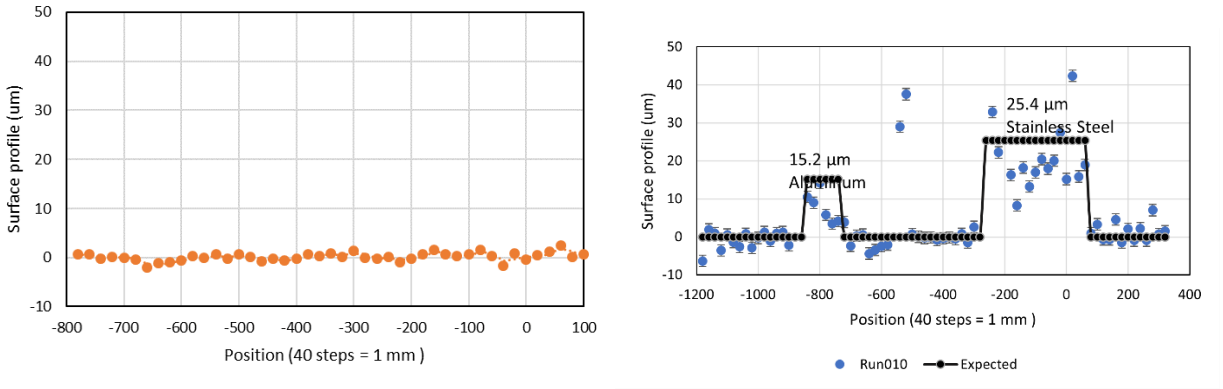

Figure 30. Diagrams of surface profile scans. Scanning across a flat steel gauge block (left). Scanning across a 15.2 µm thick aluminum foil strip and a 25.4 µm thick stainless-steel foil strip on a substrate (right).

Despite the capabilities of the profilometer, there were two main challenges when trying to measure thickness by scanning across the surface of a tin coated lithium target. First, it was suspected that tin and lithium alloys formed on the targets, as the lithium oxidized, the alloy lost its electrical conductivity which was needed for the probe on the picomotor to know when it has reached the surface of the target. Second, due to the strength property of the tin coated lithium film, the steel probe would often puncture through the film as it is harder.

Chapter 6

CONCLUSION

Even though the current deposition system is capable of depositing multi-layered films, the additional protective film layer is not successfully preventing the underlying Li film layer from oxidizing. Potential issues such as cross-contamination, substrate overheating, and the same diameter coatings were thought to explain why the additional coating did not work as expected.

The future goal is to produce Li films that can be stored in air without oxidation. As future experiments such as MTW TNSA production measurement of ^{7}Li(d, p)^{8}Li and OMEGA-60/OMEGA EP TNSA test of SLICS with ^{6}Li(t, p)^{8}Li will need Li targets. To address the mentioned issues, a new design shown in Figure 31 has been proposed. The "house" has been redesigned to include a divider between the two boats to minimize cross-contamination. Additionally, the single large opening will be replaced with respective 15.5 mm and 19.05 mm openings for Li coating and additional coating, with the center of each opening aligned directly over the center of each boat. A horizontal copper slider and heat dissipator will hold and move the substrate directly over the circular openings. This will solve the issue of non-uniform film coatings on the substrate as the substrate would be directly above the evaporant.

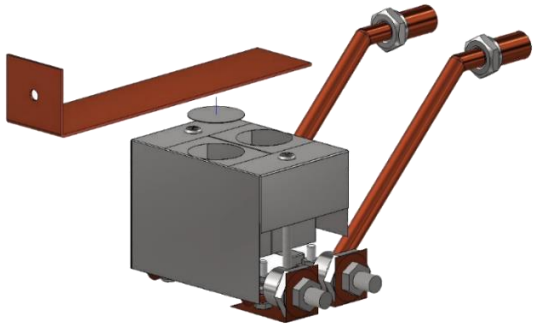

Figure 31. CAD drawing of the future evaporator design: The “house” will include a divider between the boats to prevent cross-contamination, with an opening directly over the center of each boat for more uniform film deposition. Additionally, a copper strip, serving as both a slider and a heat dissipator, will hold and move the substrate between the openings.

Appendix A

DMDTDR MAIN FUNCTION CODE FOR MASS DISTRIBUTION CALCULATION

The following code was used to numerically integrate the mass distribution integral equation as derived in Chapter 2.

```
#include<cmath>
# include<time.h>
//Defining a function that calculate the mass over the area of the ring on the substrate based on given r2 value
void DMDTDR(){
   //Defining the lower and upper bounds for each variable
   double lr1 = 0;
   double ur1 = 0.25;
   double lthe1 = 0;
   double uthe1 = 2*M_PI;
   double lthe2 = 0;
   double uthe2 = 2*M_PI;
   //Defining the number of steps
   int step = 100;
   //Finding the step size of variable with the given lower and upper bounds
   double dr1 = (double) (ur1-lr1)/step;
   double dthe1 = (double) (uthe1-lthe1)/step;
   double dthe2 = (double) (uthe2-lthe2)/step;

   int n = 310; //This is the full raduis of the substrate that the lithium would be deposited on.
         double result[n], r2[n];//Defining two arrays to contain the result with its respective r2 value.
         //These are experimentally measured thickness across three different location of a Li target.
   double measure[3] = {0.011, 0.003, 0};
         double r[3] = {0, 0.32, 0.64};
   for(int i = 0; i < n; i++){
   r2[i] = (i/1000.0);//raduis value, divided by 100 because the actual full raduis is .30cm
   if(i == 0){
      result[i]=4.84556;
   }
   else{
      result[i] = (QuadIntegral(lr1, lthe1, lthe2, step, dr1, dthe1, dthe2, r2[i]))/(2*M_PI*r2[i]);
   }
   }

   //Normalization by dividing each value by the max value of that dataset then times 100 to get the percentage
   for(int i = 0; i < n; i++){
      result[i] = (result[i]/4.84556) * 100;
   }
   for(int j = 0; j < 3; j++){
      measure[j] = (measure[j]/0.011) * 100;
   }

   //Plotting
```

```
   auto c1 = new TCanvas("c1", "Mass as function of raduis", 600, 400);
   auto mg = new TMultiGraph();// This allows me to plot different things on the same graph
   auto g = new TGraph(n, r2, result);
   g->SetName("g");
   g->SetTitle("M(r2)");
   g->SetMarkerStyle(21);
   g->SetDrawOption("AP");
   g->SetLineColor(2);
   g->SetLineWidth(4);
   g->SetFillStyle(0);
   auto g1 = new TGraph(3, r, measure);
   g1->SetName("g");
   g1->SetTitle("M(r2)");
   g1->SetMarkerStyle(21);
   g1->SetDrawOption("AP");
   g1->SetLineColor(3);
   g1->SetLineWidth(4);
   g1->SetFillStyle(0);
   mg->SetTitle("M(r2); Position(cm); Mass %");
   mg->Add(g);//Adding mutiple graphs into one graph
   mg->Add(g1);
   mg->Draw("*a f l2d");

}
```

Appendix B

PROFILOMETER OPERATION CODE

The following code was used to control the profilometer to create profile scans across thin film targets.

```
import numpy as np
import RPi.GPIO as GPIO
```

```
import gpib
import subprocess
import yaml
import time

# General Setup

# Picomoter distance per tick
PICO_ROT = (1/80)*2.54e4                # um per rotation of picomotor
PICO_DIAM = 0.8                    # diameter of picomotor wheel
ENC_DIAM = 0.5                     # diameter of rotary encoder wheel
ENC_TICKS = 360*4                       # ticks per rotsry encoder rotation
PICO_TICKS = ENC_TICKS*PICO_DIAM/ENC_DIAM   # ticks per picomotor rotation
DIST_TICK = PICO_ROT/PICO_TICKS           # distance in um per tick of rotary encoder
BACKOFF = 50                         # distance in um to back off for each translation step
BACKOFF_TICKS = int(BACKOFF/DIST_TICK)      # number of rotary endcoder ticks to back off

print("Distance in um per rotation of picomotor: ", PICO_ROT)
print("Diameter of picomotor wheel: ", PICO_DIAM)
print("Diameter of rotary encoder wheel ", ENC_DIAM)
print("Ticks per picomotor rotation: %6.2f"% PICO_TICKS)
print("Distance in um per tick of rotary encoder: %5.3f "% DIST_TICK)
print("Distance in um to back off %5.3f (%d rotary encoder ticks)"% (BACKOFF, BACKOFF_TICKS))

# set up GPIO pins for touch and rotary encoder
GPIO.setmode(GPIO.BCM)
GPIO.setup(27, GPIO.IN, pull_up_down=GPIO.PUD_UP)  # touch input with pull up resistor
GPIO.setup(2, GPIO.IN) # CW rotation ticks
GPIO.setup(3, GPIO.IN) # CCW rotation ticks

# get scan parameters from user
STEPS_MM = 40   # steps per mm for the conteroller
TAR_START = int(float(input("Stepper starting target position (mm): "))*STEPS_MM)
TRANSLATE = int(float(input("Stepper translation distance (mm): "))*STEPS_MM) # total distance to move bed (in
mm)
STEPSIZE = int(float(input("Stepper step size (mm): "))*STEPS_MM) # size of each step

# create array to store the data
profile = np.full((int(TRANSLATE/STEPSIZE+2),3),-999)  # position,istepsin,encoder,notouch

# starting encoder position
encoder_position = 0

# Define useful functions

# Stepper motor command function
def ticcmd(*args):
   return subprocess.check_output(['ticcmd'] + list(args))

#GPIB (picomotor) commend function
def cmd(con, cmd):

   Fail = 0
```

```
    Again = True

    while(Again):
        try:
            gpib.write(con,cmd)
        except gpib.GpibError:
            print("write error: ibsta = ",bin(gpib.clear(con)))
            Fail = Fail + 1
        else:
            Again = False

    Again = True

    while(Again):
        try:
            result = ""
            c = gpib.read(con,2048)
        except gpib.GpibError:
            print("read error: ibsta = ",bin(gpib.clear(con)))
            Fail = Fail + 1
        else:
            result=c.decode("utf-8")
            Again = False

    if Fail>0:
        print("gpib read/write failed ",Fail," times.")

    return result

# set up interupts to handle rotary encoder ticks
def my_callback_CW(channel):
    global encoder_position
    encoder_position = encoder_position + 1


def my_callback_CCW(channel):
    global encoder_position
    encoder_position = encoder_position - 1



# Open the gpib device
con=gpib.dev(0,1)

# Query the unit identification string
reply = cmd(con,"*IDN?\n") # send the standard SCPI identify command
print(reply)

# set up steper motor parameters
status = yaml.full_load(ticcmd('-s', '--full'))
print(status['Name'])
position = status['Current position']
print("Initial position is {}.".format(position))
```

```
ticcmd('--current',str(1500))   # set maximum current (mA)
ticcmd('--step-mode','full')    # 200 steps/rotation
                        # pitch of screw = 5 mm/rot
                        # (5 mm/rot) / (200 step/rot) = 0.025 mm/step
ticcmd('--energize')          # energize coils


################################################
# Now lets scan the profile
# move stepper to starting position
print("Return to start position {}.".format(TAR_START))
ticcmd('--exit-safe-start', '--position', str(TAR_START))
time.sleep(5)

# Scan the profile
print("\nBEGIN PROFILE SCAN.")

status = yaml.full_load(ticcmd('-s', '--full'))
start_position = status['Current position']

position=start_position
end_position=start_position+TRANSLATE
print("Start position is {}.".format(start_position))
print("End position is {}.".format(end_position))

# start the interupt handler to update rotary encoder position
GPIO.add_event_detect(2, GPIO.FALLING, callback=my_callback_CW)
GPIO.add_event_detect(3, GPIO.FALLING, callback=my_callback_CCW)

# Loop moving the stepper STEPSIZE at a time
# run picomoter in one pulse at a time
#    1 pulse = 30 nm (approx)
#    CW = in
#    CCW = out

i=0    #index for profile data array
while  (position<=end_position) :

   # Loop moving the stepper by STEPSIZE at a timelocal variable 'encoder_position' referenced before assignment

   # run picomoter in one pulse at a time
   #    1 pulse = 30 nm (approx)
   #    CW = in
   #    CCW = out

   # Set direction move in = rotate CW
   reply = cmd(con,"SOUR:DIR CW\n")
   print('Move in -- set to CW: ' + reply)
   reply = cmd(con,"SOUR:DIR ?\n")
   #print('Read back direction: ' + reply)

   NOTOUCH = GPIO.input(27)
```

```
    istepsin = 0
    old_encoder = encoder_position

    while (NOTOUCH):
        reply = cmd(con,"SOUR:PULSE:COUN 1\n")
        NOTOUCH = GPIO.input(27)
        istepsin = istepsin + 1;
        if (encoder_position != old_encoder):
            #print("steps_in=",istepsin," encoder=",encoder_position,NOTOUCH)
            istepsin = 0
            old_encoder = encoder_position

    #print("steps_in=",istepsin," encoder=",encoder_position,NOTOUCH)

    # Set direction move  out = rotate CCW
    reply = cmd(con,"SOUR:DIR CCW\n")
    print('Move out -- set to CCW: ' + reply)
    reply = cmd(con,"SOUR:DIR ?\n")
    #print('Read back direction: ' + reply)

    NOTOUCH = GPIO.input(27)
    istepsout = 0
    old_encoder = encoder_position

    while (encoder_position < old_encoder+BACKOFF_TICKS):
        reply = cmd(con,"SOUR:PULSE:COUN 1\n")
        istepsout = istepsout + 1;

    #print("steps_out=",istepsout," encoder=",encoder_position)

    #print("Translating...")

    profile[i]=[position,old_encoder,encoder_position]
    print(position,old_encoder,encoder_position)
    i = i + 1

    movetoposition=position+STEPSIZE
    #print("Moving to position {}.".format(movetoposition))
    ticcmd('--exit-safe-start', '--position', str(movetoposition))

    while position !=  movetoposition:
        status = yaml.full_load(ticcmd('-s', '--full'))
        position = status['Current position']
        #print("Current position is {}.".format(position))

time.sleep(5)

status = yaml.full_load(ticcmd('-s', '--full'))
position = status['Current position']
print("Current position is {}.".format(position))

print(profile)
gpib.close(con)
```

References

[1] Mark Yuly, Stephen Padalino, Adam Brown, Andrew Hotchkiss, Chunsun Lei, Andrew Martin, "Trapping and detecting trace radioactive isotopes produced in ICF implosions," in Nuclear and Plasma Diagnostics for the EP-OMEGA and MTW Laser Systems, LLE Proposal for Subaward 416231-G, 2022 (unpublished).

[2] Mark Yuly, Stephen Padalino, Noah Harley, Andrew Hotchkiss, Chunsun Lei, Andrew Martin. "A new technique for measuring light ion nuclear reactions using TNSA," in Nuclear and Plasma Diagnostics for the EP-OMEGA and MTW Laser Systems, LLE Proposal for Subaward 416231-G, 2023 (unpublished).

[3] W. R. Grove, Phil. Trans. Roy. Soc., London A **142**, 87 (1852).

[4] M. Faraday, Phil. Trans. **147**, 145 (1857).

[5] D. M. Mattox, Handbook of Physical Vapor Deposition (PVD) Processing 2rd Edition, William Andrew (2010).

[6] R. D. Harbison, M. M. Bourgeois, G. T. Johnson, *Hamilton and Hardy's Industrial Toxicology 6th Edition*, Wiley p. 141-148 (1934).

[7] Abner Brenner, "Magnetic Method for Measuring the Thickness of Nonmagnetic Coatings on Iron and Steel," Journal of Research of the National Bureau of Standards, **20**, 357-358 (1938).